Biointerface Research in Applied Chemistry
Open-Access Journal (ISSN: 2069-5837)

Article
Volume 16, Issue 3, 2026, 99
https://doi.org/10.33263/BRIAC163.099

Exploring Anti-Aging Potential of Flavonoids from *Muntingia calabura* Fruit Extract: LC-ESI/MS, Network Pharmacology, and Molecular Validation

Syamsu Nur [1,*], Batari Novia Sari [1], Fitriyanti Jumaetri Sami [1], Nursamsiar [1], Lusi Agus Setiani [2], Asril Burhan [3], Ismail [4], Marwati [3], Nur Khairi [4], Nita Triadisti [5], Desy Muliana Wenas [6]

[1] Department of Pharmaceutical Analysis and Medicinal Chemistry, Almarisah Madani University, Makassar City, Indonesia; syamsunur@univeral.ac.id (S.N.); fitriyantijumaetri@univeral.ac.id (F.J.S.); nursamsiar@univeral.ac.id (N.);
[2] Pharmacy Study Program, Pakuan University, Bogor, West Java, Indonesia; lusi.setiani@unpak.ac.id;
[3] Department of Pharmaceutical Biology, Almarisah Madani University, Makassar City, Indonesia; asrilburhan@univeral.ac.id (A.B.); marwati@univeral.ac.id (M.);
[4] Department of Pharmaceutical Technology and Pharmaceutical, Almarisah Madani University, Makassar City, Indonesia; ismail@univeral.ac.id (I.); nurkhairi@univeral.ac.id (N.K.);
[5] Department of Biology Pharmacy, Faculty of Pharmacy, Universitas Muhammadiyah Banjarmasin, Banjarmasin, 70115, Indonesia; triadisti@umbjm.ac.id;
[6] Faculty of Pharmacy, National Institute of Science and Technology, Jakarta 12630, Indonesia; desywenas@istn.ac.id;
* Correspondence: syamsunur@univeral.ac.id;

Received: 31.07.2025; Accepted: 17.12.2025; Published: 15.06.2026

Abstract: *Muntingia calabura* L. has been reported to possess diverse pharmacological effects, with flavonoid derivatives recognized as the main bioactive constituents. This study aimed to identify flavonoids from *M. calabura* fruit extract and to explore their pharmacological potential as anti-aging agents targeting key proteins through a network pharmacology approach and in silico analyses. The research was conducted in several stages, including maceration extraction and identification of flavonoid compounds from the ethanol extract of *M. calabura* fruit. The identified compounds were subsequently evaluated for physicochemical properties and skin permeability using web-based tools. Compounds meeting these criteria were further analyzed through network pharmacology, molecular docking, and molecular dynamics simulations. A total of 41 compounds were identified, including 36 flavonoid derivatives. Among them, 6-hydroxy-7-methoxy-2-(2-phenylethyl)-chromone (compound 16) demonstrated strong multi-target interactions with aging-related proteins, including collagenase, gelatinase, elastase, and tyrosinase. Physicochemical and skin permeability evaluations indicated that 38 compounds were suitable for further analysis, while network pharmacology linked 19 compounds to aging-related proteins, particularly matrix metalloproteinases (MMPs) and tyrosinase (TYR). Docking studies revealed that compound 16 exhibited binding affinities of –8.65 kcal/mol (collagenase), –8.91 kcal/mol (gelatinase), –7.26 kcal/mol (elastase), and –1.31 kcal/mol (tyrosinase). Molecular dynamics simulations confirmed the stability of these interactions. Collectively, these findings suggest that the ethanol extract of *M. calabura* fruit may exert anti-aging effects, supported by the presence of stable, multi-target flavonoid derivatives, making it a promising candidate for further research and development.

Keywords: anti-aging; homoisoflavonoid; iMODS; Jamaican cherry; matrix metalloproteinases; molecular docking; molecular dynamics; network pharmacology.

1. Introduction

Skin aging is a natural process influenced by various intrinsic and extrinsic factors. Over time, the skin undergoes structural and functional changes, leading to visible signs such as wrinkles, fine lines, and loss of elasticity [1]. The molecular mechanisms of skin aging through enzyme inhibition pathways can generally occur through several pathways, including Matrix Metalloproteinase (MMP), Elastase, tyrosinase, and Hyaluronidase [2]. The enzymatic pathway is one of the aging targets modulated by the accumulation of increased Reactive Oxygen Species (ROS), which activates the mitogen-activated protein kinase (MAPK) pathway. This pathway will affect regulatory proteins, namely Transforming Growth Factor Beta (TGF-β) and Activator Protein 1 (AP-1). TGF-β induces tissue formation in the extracellular matrix, such as collagen and elastin. Meanwhile, AP-1 works by degrading extracellular matrix proteins, damaging collagen and elastin tissue, which, over time, can cause premature skin aging. AP-1 will induce the activity of skin-degrading enzymes such as collagenase, gelatinase, elastase, and hyaluronidase [2–5]

Collagenase proteins, especially matrix metalloproteinase-1 (MMP-1), and gelatinase proteins, such as matrix metalloproteinase-9 (MMP-9), play an essential role in the degradation of collagen and other components of the extracellular matrix in the skin. Increased MMP activity can lead to loss of skin firmness, increased wrinkles, and decreased elasticity [6]. MMP-1 protein, in particular, is responsible for destroying fibrillar collagen fibers, such as type I and type III, which maintain the structural integrity and elasticity of the skin. MMP-9 also contributes to the degradation of gelatin, type IV collagen, and other components of the extracellular matrix [7]. Increased gelatinase activity can result in fragmentation of the extracellular matrix, the skin's inability to maintain structural strength, and increased risk of wrinkles and skin sagging [5,8].

The same thing also happens to elastin tissue. Elastase degradation occurs due to the overexpression of other skin-degrading enzymes, such as elastase. Elastase activity increases with age by degrading elastin tissue in the dermis, which causes a decrease in the skin's elastic properties and an increase in the expression of matrix metalloproteinases (MMPs) due to UV rays that damage elastin tissue and accelerate the skin aging process [9–11]. Hyaluronidase degrades hyaluronic acid, thereby impairing hydration, firmness, and skin elasticity and, consequently, accelerating the development of wrinkles and other aging-related manifestations. Exposure to external factors of UV rays also increases hyaluronidase activity [12].

Beyond its biological dimension, skin aging represents a major public health and socioeconomic concern. Demographic projections indicate that the proportion of the global population aged 60 years and above will nearly double from 12% in 2015 to 22% by 2050. This demographic shift is accompanied by reduced quality of life and heightened demand for effective interventions. In parallel, the global anti-aging skincare market exceeded USD 60 billion in 2022 and is projected to surpass USD 90 billion by 2030, underscoring the urgency of identifying safe, natural, and scientifically validated anti-aging agents [13,14].

The production of various active ingredients that can be used as anti-aging agents must be explored comprehensively. The primary approach is to develop abundant natural resources to serve as effective raw material candidates for anti-aging. One plant that can be utilized is the Kersen (*Muntingia calabura* L.) plant. *Muntingia calabura*, commonly referred to as Kersen in Indonesia, is a tropical tree species that has a rich history of use in traditional medicine across various countries [15,16]. Previous research has demonstrated the pharmacological properties

of *M. calabura*, particularly its fruit, which shows promising anti-aging and antioxidant capabilities. The study suggests that *M. calabura* fruit may function as an anti-aging agent by reducing oxidative stress or through enzymatic pathways [17–19]. These results provide a foundation for further investigation into specific chemical components, thereby shedding light on the potential mechanisms of action of *M. calabura* fruit.

However, systematic investigations into its secondary metabolites, particularly flavonoids, remain limited. While compounds such as rutin and quercetin have been identified in related species, the specific flavonoid composition of *M. calabura* fruit extract has not been comprehensively reported. Moreover, most existing studies focus on broad antioxidant outcomes without elucidating the molecular mechanisms underlying these effects, such as modulation of ROS-scavenging enzymes, regulation of collagen-degrading matrix metalloproteinases (MMPs), or activation of signaling pathways linked to skin aging [19]. This gap underscores the need to target the exploration of unreported flavonoid constituents and their mechanistic roles in anti-aging activity. By characterizing the flavonoid profile of *M. calabura* fruit extract and investigating its potential pathways of action, this study provides novel insights into the bioactive compounds responsible for its pharmacological benefits.

In this study, ethanol was selected as the extraction solvent due to its broad polarity range, safety profile, and ability to solubilize diverse phytochemicals, including both polar and moderately non-polar compounds. Although Nur *et al*. reported that the ethyl acetate fraction of *M. calabura* exhibited slightly higher antioxidant activity than the ethanol extract, the difference was not statistically significant [17]. Moreover, ethanol extraction reported higher yields, ensuring broader recovery of phytochemicals and greater feasibility for pharmacological exploration [17,19]. This rationale supports the use of ethanol to obtain a comprehensive representation of the fruit's phytochemical diversity, enabling identification of multiple bioactive compounds that may act synergistically in multitarget mechanisms relevant to skin aging. Thus, ethanol complements previous findings by providing a holistic extract suitable for advanced analyses such as network pharmacology, molecular docking, and molecular dynamics.

Despite previous reports on the antioxidant and anti-aging potential of *M. calabura* fruit, most studies have focused on general bioactivity rather than detailed characterization of its secondary metabolites. Specific flavonoid derivatives remain underexplored, and their molecular pathways—particularly multitarget interactions with collagenase, gelatinase, elastase, and tyrosinase—are not yet elucidated. This study, therefore, addresses a critical research gap by systematically identifying flavonoid derivatives from *M. calabura* fruit extract and integrating computational approaches to clarify their mechanisms of action. Furthermore, this multi-component strategy aligns with a new drug discovery paradigm that emphasizes safety, low toxicity, and therapeutic benefits, reinforcing the relevance of *M. calabura* as a potential anti-aging agent.

2. Materials and Methods

2.1. Materials.

The part of the *M. calabura* plant used in this study was a ripe greenish-red fruit collected from the Biringkanaya District in Makassar City, South Sulawesi, Indonesia (-5.11312, 119.513806). The sample was characterized in the Pharmaceutical Biology Laboratory at Almarisah Madani University to evaluate the clarity of the plant species. It was

identified as Kersen fruit from the Muntingiaceae family, classified as *Muntingia calabura* L., with the specimen number 0528/U/B/2023.

2.2. Preparation of dried samples of M. calabura fruit.

The *M. calabura* fruit was wet sorted to remove impurities or other unwanted materials. Additionally, it was washed with running water to eliminate any impurities attached to the fruit. Next, it was chopped into small pieces to optimize the drying process and then dried in an oven at 40°C. Dry sorting was performed after drying, followed by smoothing and sieving with a mesh size of 40, after which the weight of the dried sample was recorded [20].

2.3. Extract preparation.

The dry powder of *M. calabura* fruit was then macerated using a 70% ethanol solvent at a ratio of 1:10. The dry powder was placed into a maceration vessel, wetted for 30 minutes, and then the remaining solvent was added until all the dry samples were submerged. The vessel was then covered and soaked for 24 hours, stirring every 6 to 12 hours. The filtrate and residue were separated on filter paper, and the resulting separation was then concentrated and evaporatedsing a rotary evaporator [20,21].

2.4. Secondary metabolite profile by LC/MS-QTOF analysis.

Compounds from *M. calabura* fruit extract were predicted using the LC/MS-QTOF method. This analysis followed the procedure outlined by Qiao *et al*. [22]. Liquid Chromatography was linked to Mass Spectrometry Q-TOF, which was equipped with an Electrospray Ionization (ESI) source. LC/MS-QTOF was employed to acquire all metabolite fingerprints from the sample. In ESI mode, the full scan was configured for m/z from 50 to 1200 Da. Separation occurred at a temperature of 40°C on a C18 Aquity UPLC HSS T3 100A 2.1 mm × 100 mm, 1.8 µm column, with a mobile phase consisting of (A) 10:90 (v/v) formic acid/acetonitrile (ACN) and (B) 10:90 (v/v) formic acid/aquabidestillata. The selection of these solvent systems was intended to optimize ionization efficiency and chromatographic separation of diverse phytochemicals. Formic acid was included to enhance protonation and improve peak resolution, while acetonitrile and aquabidestillata provided complementary polarity ranges to ensure broader metabolite coverage. The sample extract was filtered through a 0.22 µm GHP/PTFE membrane filter and transferred to a specialized vial. The injection volume was 10 µL, the flow rate was set at 0.6 mL/min, and the autosampler temperature was kept at 15°C. Mass spectrometry functioned in positive (+) and negative (−) electrospray ionization (ESI) modes. Secondary metabolite screening included profiling, identification, and confirmation using a QTOF mass spectrometer from Waters, specifically the Xevo G2-S QTOF-MS/MS. Additionally, identification was accomplished using the mass spectrum database of organic compounds in the UNIFI Scientific Information System data library [11].

2.5. In silico prediction of physicochemical properties, skin permeability, and topical toxicity of identified compounds.

Physicochemical values were calculated according to Lipinski's rule, which includes molecular weight, log P, hydrogen bond donors, hydrogen bond acceptors, and molar refraction using the HyperChem Professional® v.8.00 software package and the SwissADME web tool (http://www.swissadme.ch/). Skin permeability predictions were made using Web Tools from

PreADMET 2.0 [23]. Meanwhile, toxicity predictions were performed using Web Tools from ADMETlab 3.0 (http://scbdd.com/) with Eye Irritation and Skin Sensitization parameters, and admetSAR 3.0 (https://lmmd.ecust.edu.cn/admetsar3/resource.php) for Skin Irritation parameters [24].

2.6. Network pharmacology analysis.

Compounds successfully identified from LC/MS-QTOF exhibit favorable in silico physicochemical properties. Therefore, an identification search was conducted, and the SDF file for the compound was downloaded from PubChem. The target protein for the compound was then located using bindingdb.com. After identifying the target, the next step is to obtain information on the gene and its associated disease via disgenet.org. The gene pathway can be examined using the KEGG pathway, and subsequent construction can be accomplished through the Cytoscape network of the gene compound and its pathway [25].

2.7. Docking molecular analysis.

2.7.1. Ligand structure preparation.

Ligand preparation begins with creating a 2D structure using the ChemDraw Ultra 8.0 program within the ChemOffice v.8.0 package, followed by the construction of a 3D ligand structure using Chem3D v.8.0, also part of the ChemOffice v.8.0 package, and saved in (.mol) file format. The 3D structure was subsequently geometry-optimized using the HyperChem 8.0.10 software package. Geometry optimization was performed by adding hydrogen atoms and constructing a model, followed by semi-empirical calculations using the AM1 force field in the HyperChem 8.0.10 program package, with an RMS gradient value of 0.001. The optimized ligand structure was then analyzed for its molecular properties and saved in a (.hin) file format, which is subsequently converted into a (.pdb) file format using the ArgusLab v4.0.1 program package for further use in the AutoDock Tools v1.5.7 program package. Using the AutoDock Tools v1.5.7 program package, the ligand compound was assigned all hydrogen bonds. Then, the Compute Gasteiger and Merge Non-Polar Hydrogens options were selected, and the file was saved in (.pdbq) format. This is followed by Torsion input, which specifies the number of torsions, selects the fewest atoms, and saves the result in (.pdbqt) format [26,27].

2.7.2. Molecule target preparation.

The 3D structures of each protein—Collagenase, Gelatinase, Elastase, and tyrosinase—were displayed as ligands in the BIOVIA Discovery Studio Visualizer v24.1.0.23298 program, used for visualizing molecular docking results. Among the target proteins, Collagenase, Gelatinase, and tyrosinase are dimers consisting of Chain A and Chain B. For the same sequence and chain, Chain A was selected and further prepared using AutoDock Tools v1.5.7, whereas Elastase consists of only one chain (Chain A). To conduct molecular docking studies on the selected structure, water molecules were first removed, and the native ligand was saved in a (.pdb) file, which was treated as a receptor. Next, polar hydrogen atoms were added to the structural protein, and the four zinc ions (Zn^{2+}) and three calcium ions (Ca^{2+}) were removed from the Collagenase protein complex. In comparison, the four calcium ions (Ca^{2+}) and two zinc ions (Zn^{2+}) were removed from the Gelatinase protein complex. The partial charges of each atom for both proteins were calculated using the Kollman algorithm, which is included in

the AutoDock Tools v1.5.7 program package. Then, the Chain A structure was saved in a .pdbqt format file [26–28].

2.7.3. Docking simulation.

Docking was performed using the AutoDock Tools v1.5.7 program. The grid was created with dimensions and coordinates corresponding to the grid box (x, y, z) for each target protein, encompassing all amino acid residues involved in ligand binding. This grid was established at the location of the bound ligand structure. Information regarding the target protein and grid dimensions was then stored in a (.gpf) format file. The electrostatic potential map and calculation results were saved in a (.glg) format file. Next, the docking tool was selected, and the Lamarckian Algorithm was used to save the results in a (.dpf) format file. The docking simulation results were stored in a (.dlg) format. The evaluation parameters include ligand structure orientation, hydrogen-bonding interactions, free energy values, and inhibition constants from the molecular dockingf each ligand [26–28].

2.8. Molecular dynamic simulation by the iMODS server.

Molecular dynamics (MD) analysis using the Integrated Modeling of Dynamic Systems (iMOD) server is a way to study molecular motion and interactions over time [29,30]. The steps in molecular dynamics analysis using iMOD include preparing the ligand-protein complex from the previous optimization and docking analysis. The ligand-protein complex was saved as a file (.pdb). It was then uploaded to the website https://imods.iqfr.csic.es/. Next, the simulation parameters were configured, including root mean square fluctuation (RMSF) using https://biocomp.chem.uw.edu.pl/CABSflex2 and the parameters of deformability against index atoms, B-factor against index atoms, index residue matrix, eigenvalue against index mode, and percentage of variance against index mode were visualized by https://imods.iqfr.csic.es/. After setting all parameters, the simulation was run. The iMOD server performs the calculations in the background, and then the analysis results can be viewed [31].

3. Results and Discussion

3.1. Phytochemical analysis.

The secondary metabolic content of *M. calabura* fruit extract was analyzed using the LC/MS-QTOF method. Figure 1 shows a chromatogram of the successfully identified compounds. Based on confirmation results for its chemical structure (Mass Candidate) in the UNIFI database, 41 compounds have been identified in *M. calabura* fruit extract, as shown in Table 1.

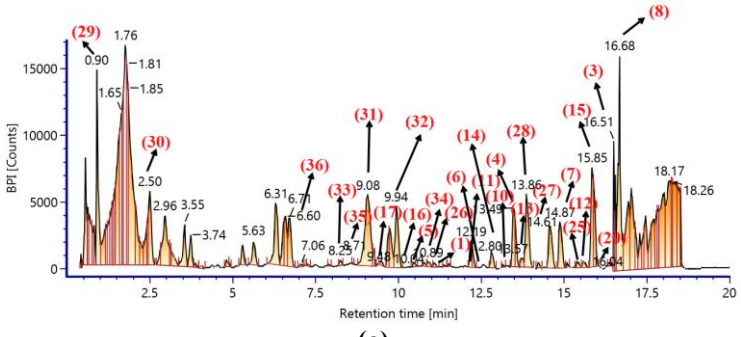

(a)

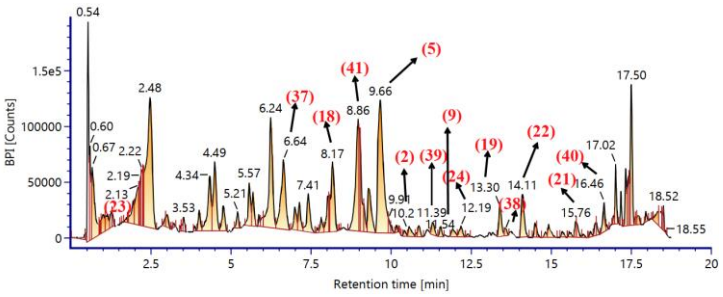

(b)

Figure 1. LC/MS-QTOF Spectrum of *M. calabura* fruit ethanol extract, integrated spectrum in **(a)** ESI positive (+) mode; **(b)** ESI negative (-) mode. The chemical compound names are listed in the order presented in Table 1.

Table 1. Chemical compounds, molecular weight, and group compounds prediction of the ethanolic extract of *M. calabura* fruit.

Comp. code	Compounds	Observed RT (min)	Molecular weight (Da)	Ionization *(m/z)*	Compounds group	Class of compounds
1	1,5-Dihydroxy-2,3,4,7-tetramethoxyxanthone	11.39	349.0907	M+H	Flavonoid	Xanthone
2	2,5-Dimethyl-1,4-benzoquinone	10.22	137.0589	M-H	Quinoids	Quinoids
3	2,5,7-Trihydroxy-6,8-dimethyl-3-(3',4'-methylenedioxybenzyl) chroman-4-one	16.53	359.1125	M+H	Flavonoid	homoisoflavonoid
4	2,5,7-Trihydroxy-6,8-dimethyl-3-(4'-methoxybenzyl) chroman-4-one	13.49	345.1335	M+H	Flavonoid	Homoisoflavonoid
5	2"-O-Feruloylaloesin	9.66	569.1639	M-H	Phenolic	Phenolic
6	2′-Hydroxy-4′,6′-dimethoxydihydrochalcone	12.2	287.1276	M+H	Flavonoid	Chalcone
7	2′,7-Dihydroxy-4′,5′-dimethoxyisoflavone	14.87	315.085	M+H	Flavonoid	Isoflavonoid
8	3,8-Dihydroxy-4,10-dimethoxy-7-oxo-[2] benzopyrano[4,3-b] [1]benzopyran-7-(5H)-one	16.68	343.0811	M+H	Flavonoid	Xanthone
9	3',5',β-Trihydroxy-3,4,4',α-tetramethoxychalcone	11.54	375.1054	M-H	Flavonoid	Chalcone
10	3′-O-Angeloylhamaudol	13.28	359.1487	M+H	Flavonoid	Pyranochromenes
11	4',5,6,7-Tetramethoxy-flavone	12.13	341.1039	M+H	Flavonoid	Flavon
12	5-Hydroxy-7,8-dimethoxy-6-methyl-3-(3',4'-dihydroxybenzyl) chroman-4-one	15.6	361.1281	M+H	Flavonoid	Homoisoflavonoid
13	5,7-Dihydroxy-6-methoxyl-8-methyl-3-(2′,4′-dihydroxybenzyl) chroman-4-one	13.57	347.1126	M+H	Flavonoid	Homoisoflavonoid
14	5,7,4′-Trimethoxyflavone	12.8	313.1059	M+H	Flavonoid	Flavon
15	5,7,8,3'-Tetrahydroxy-3,4'-dimethoxy flavone	15.85	347.0751	M+H	Flavonoid	Flavon
16	6-Hydroxy-7-methoxy-2-(2-phenylethyl) chromone	10.04	297.112	M+H	Flavonoid	Chromone
17	6-Methoxy-2-[2-(3'-methoxyphenyl) ethyl] chromone	9.48	311.1279	M+H	Flavonoid	Chromone
18	Aloeresin A	8.1	539.1559	M-H	Flavonoid	Cinnamate ester
19	Amaranthin	13.3	725.1698	M-H	Alkaloid	Alkaloid
20	Bavachromene	16.04	323.1272	M+H	Flavonoid	Chalcone
21	Dichotomitin	15.77	357.0606	M-H	Flavonoid	Homoisoflavonoid
22	Eupatin	14.11	359.0762	M-H	Flavonoid	Flavon
23	Gentianamine	1.65	204.0656	M-H	Alkaloid	Alkaloid
24	Hispidulin 7-(6-E-p-coumaroyl-β-D-glucopyranoside)	12.19	607.143	M-H	Flavonoid	Flavon
25	Isoneobavachalcone	15.42	299.0909	M+H	Flavonoid	Chalcone
26	Kaempferol	10.92	287.0541	M+H	Flavonoid	Flavonol
27	Leachianone G	14.61	357.1328	M+H	Flavonoid	Flavanone
28	Licoflavone A	13.86	323.1277	M+H	Flavonoid	Flavon
29	Mahuannin A	0.90	543.1328	M+H	Flavonoid	Flavanols
30	Maltol	2.51	127.0386	M+H	-	-
31	Methyl ophiopogonone A	9.08	341.1016	M+H	Flavonoid	Homoisoflavonois
32	Morin	9.94	303.0497	M+H	Flavonoid	Flavonol

Comp. code	Compounds	Observed RT (min)	Molecular weight (Da)	Ionization *(m/z)*	Compounds group	Class of compounds
33	Myricetin	8.25	319.0437	M+H	Flavonoid	Flavonol
34	Nevadensin-5-O-β-D-glucoside	10.48	507.1488	M+H	Flavonoid	Flavon
35	Nobiletin	8.7	403.1357	M+H	Flavonoid	Flavon
36	Ophiopogonanone B	6.60	315.1223	M+H	Flavonoid	Homoisoflavonoid
37	Pelargonidin 3-glucoside	6.45	467.072	M-H	Flavonoid	Antosianin
38	Procyanidin B2 gallate	13.52	881.1567	M-H	Flavonoid	Flavanols
39	Quercetagetin-6,7,3',4'-tetramethyl ether	11.39	373.0905	M-H	Flavonoid	Flavonols
40	Quercetin-3-O-glucuronide 6″-methylester	16.46	491.0836	M-H	Flavonoid	Flavon
41	Quercetin-6-O-glucoside	6.71	481.0981	M-H	Flavonoid	Flavonols

The compound prediction data in Table 1 show that 36 compounds from the flavonoid group were mainly identified in the ethanol extract of *M. calabura* fruit. Classification of compounds from identified flavonoids includes xanthone derivatives **(1)** and **(8)**; anthocyanin compounds **(37)**; flavone compounds **(11)**, **(14)**, **(15)**, **(22)**, **(24)**, **(34)**, **(35)**, and **(40)**; flavonol compounds **(26)**, **(32)**, **(33)**, **(38)**, **(39)**, and **(41)**; flavanone compounds **(27)**; flavonol **(29)**; homoisoflavonoid compounds **(2)**, **(3)**, **(4)**, **(12)**, **(13)**, **(21)**, **(31)**, and **(36)**; isoflavonoid compounds **(7)**; and other flavonoids such as chromone **(16)** and **(17)**; chalcone **(6)**, **(9)**, **(20)**, and **(25)** and cinnamate ester **(18).** Besides those compounds, three other groups of compounds were also identified, including phenol, such as 2''-O-Feruloylaloesin **(5)**, and Maltol **(30)**, quinoid compounds such as 2,5-Dimethyl-1,4-benzoquinone **(2)**, and others, as well as alkaloids like Amaranthin **(19)** and Gentianamine **(23).** Several previous studies have reported that extracts from various parts of the *M. calabura* plant, including leaves, roots, and stems, contain numerous flavonoid derivative compounds. These flavonoid compounds in the leaves, roots, and stems were identified as hydroxychalcones, including hydroxymethoxychalcone, methoxyflavone, hydroxymethoxyflavone, methoxyflavan, coumarin, and others[15,16,32]. However, reports based on earlier research findings related to secondary metabolites in *M. calabura* fruit extracts remain limited. Nevertheless, in general, the LC-ESI/MS analysis of the ethanol extract of *M. calabura* fruit revealed compounds similar to flavonoid derivatives previously reported in various parts of the plant. Figure 2 shows the molecular structures of the compounds successfully identified from the fruits of *M. calabura*.

Flavonoid derivatives found in the ethanol extract of *M. calabura* fruit have been reported to possess various pharmacological activities, including those listed in Table 2. These compounds typically act as antioxidants, antibacterials, antifungals, antidiabetics, anti-inflammatories, antiosteoporotics, anticancer agents, immunomodulators, hepatoprotectives, antiallergens, neuroprotectives, antimalarials, anti-aging agents, whitening agents, and brightening agents. Out of the 38 flavonoid derivative compounds with studied bioactivity, only three have been identified as having anti-aging effects through various pathways. Among these, Aloeresin A **(18)**, Morin **(32)**, and Myricetin **(33)** are specifically reported to possess anti-aging properties [33–35]. Although there are limited scientific reports on compounds in *M. calabura* fruit with anti-aging effects, further research is needed to explore their potential as anti-aging agents.

The flavonoid derivatives identified in *M. calabura* extract generally exhibit antioxidant activity; thus, their mechanisms may be related to the prevention of premature aging, either directly or indirectly. The antioxidant activity of these compounds plays a crucial role in anti-aging processes [80]. It is understood that various internal and external factors

contribute to premature skin aging. One external factor is exposure to UV rays, which can increase Reactive Oxygen Species (ROS) and lead to early skin aging.

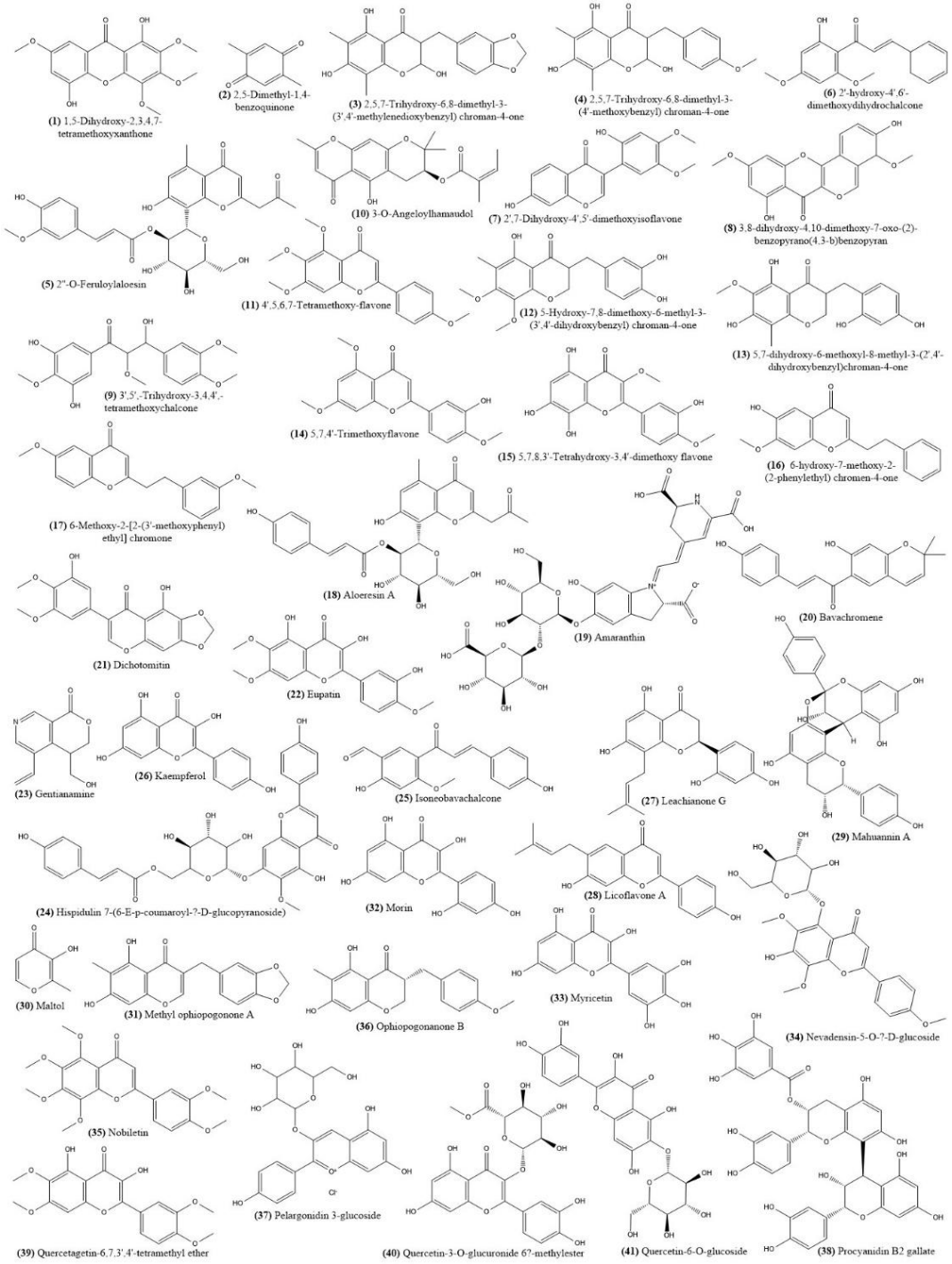

Figure 2. Molecular structure of compounds identified from *M. Calabura* fruit extract.

Table 2. Investigation of the pharmacological effects of compounds identified from the *M. calabura* fruit extract based on prior research findings.

Comp. code	Compounds	Pharmacology effect	References
1	1,5-Dihydroxy-2,3,4,7-tetramethoxyxanthone	Antioxidant, Protective effects against liver injury, Immuno-modulatory	[36–38]
2	2,5-Dimethyl-1,4-benzoquinone	Antifungal activity	[39]
3	2,5,7-Trihydroxy-6,8-dimethyl-3-(3',4'-methylenedioxybenzyl) chroman-4-one	Antioxidant	[40]
4	2,5,7-Trihydroxy-6,8-dimethyl-3-(4'-methoxybenzyl) chroman-4-one	Antioxidant	[40]
5	2''-O-Feruloylaloesin	Antioxidant and Antimycoplasmic activity	[33]

Comp. code	Compounds	Pharmacology effect	References
6	2′-Hydroxy-4′,6′-dimethoxydihydrochalcone	Anti-diabetic and Breast Cancer Cell Inhibition	[41,42]
7	2′,7-Dihydroxy-4′,5′-dimethoxyisoflavone	Anti-inflammation and anti-allergic activity	[43]
8	3,8-Dihydroxy-4,10-dimethoxy-7-oxo-[2] benzopyrano[4,3-b] [1]benzopyran-7-(5H)-one	-	-
9	3',5',β-Trihydroxy-3,4,4',α-tetramethoxychalcone	-	-
10	3′-O-Angeloylhamaudol	Anticancer activity	[44]
11	4',5,6,7-Tetramethoxy-flavone	CYP inhibitory effect	[45]
12	5-Hydroxy-7,8-dimethoxy-6-methyl-3-(3',4'-dihydroxybenzyl) chroman-4-one	-	-
13	5,7-Dihydroxy-6-methoxyl-8-methyl-3-(2′,4′-dihydroxybenzyl) chroman-4-one	Antioxidant and antibacterial activity	[46,47]
14	5,7,4′-Trimethoxyflavone	Antifungal activity	[48]
15	5,7,8,3'-Tetrahydroxy-3,4'-dimethoxy flavone	Protective Effect against AAPH-Induced Erythrocyte Hemolysis	[49]
16	6-Hydroxy-7-methoxy-2-(2-phenylethyl) chromone	-	-
17	6-Methoxy-2-[2-(3'-methoxyphenyl) ethyl] chromone	-	-
18	Aloeresin A	Anti-tyrosinase, anti-diabetic, and anti-bacterial activity	[50–52]
19	Amaranthin	Antioxidant, anti-hyperglycemic, antibacterial, hepatoprotective effect	[53]
20	Bavachromene	Antibacterial and Anti-Alzheimer effect	[54,55]
21	Dichotomitin	Anti-osteoporosis effect	[56]
22	Eupatin	Anti-inflammation and anti-Coronavirus	[57,58]
23	Gentianamine	Anti-inflammation, cytotoxic effect, anti-bacterial, immunomodulator	[59]
24	Hispidulin 7-(6-E-p-coumaroyl-β-D-glucopyranoside)	-	-
25	Isoneobavachalcone	Anticancer, antibacterial, anti-fungal, anti-inflammatory, antiviral, neuroprotective, and bone-protective activities	[60]
26	Kaempferol	Neuroprotective, immunomodulatory, and anti-inflammatory effects	[61,62]
27	Leachianone G	Anti-inflammation effect	[63]
28	Licoflavone A	Anti-ulcer and anti-inflammation	[64]
29	Mahuannin A	-	-
30	Maltol	Protective effect and anti-microbial activity	[65,66]
31	Methyl ophiopogonone A	Protective effect against Cerebral Ischemia	[67]
32	Morin	Antioxidant, anti-diabetic, anti-inflammatory, antitumoral, and neuroprotective effects, and skin protection	[34,68]
33	Myricetin	Antioxidant, anti-inflammation, anti-diabetic, anti-cancer, anti-infection, protective effect, anti-aging activity	[35,69]
34	Nevadensin-5-O-β-D-glucoside	hCE1 inhibitors	[70]
35	Nobiletin	Antioxidant, anti-inflammatory, anti-cancer, neuroprotective, and antiangiogenic activity	[71]
36	Ophiopogonanone B	Antioxidant, anti-cancer, and anti-inflammatory effects	[71–73]
37	Pelargonidin 3-glucoside	Antioxidant and anti-inflammation	[74]
38	Procyanidin B2 gallate	Suppresses production of TNF-α and IFN-γ	[75]
39	Quercetagetin-6,7,3',4'-tetramethyl ether	Antioxidant, anti-cancer, and anti-malaria effects	[76]
40	Quercetin-3-O-glucuronide 6″-methylester	Anti-inflammation and neuroprotective effect	[77,78]
41	Quercetin-6-O-glucoside	Antioxidant activity	[79]

The antioxidant ability of flavonoids can inhibit the increase of ROS, preventing the ongoing process of premature aging in various molecular pathways. For example, it can modulate the MAPK pathway, which can activate the production of extracellular matrix proteins through the Activator Protein 1 (AP-1) pathway. This activation can lead to the

stimulation of skin-degrading enzymes like matrix metalloproteinase (MMP) and tyrosine kinase. Additionally, the angiogenesis pathway can trigger the increase of other skin-degrading enzymes, such as elastase, which can worsen wrinkle formation and reduce skin elasticity [81,82]. To clarify the molecular mechanisms of the compounds identified from the ethanol extract of *M. calabura* fruit as anti-aging agents, this study used a network pharmacology approach and molecular structure analysis, including molecular docking, as alternative methods.

3.2. Physicochemical properties and skin permeability characteristics of identified compounds.

The physicochemical properties of a compound influence its characteristics and pharmacological effects. A compound is considered to have good attributes if it meets five key parameters known as the five rules, including molecular weight, Hydrogen Bond Acceptor, Hydrogen Bond Donor, Molar Refractivity, and polarity (mlog P). Meeting these physicochemical criteria provides essential information for understanding the mechanics of pre-formulation and formulation of the dosage form, ensuring effective delivery and bioavailability [28].

Molecular weight influences a compound's ability to pass through cell membranes via passive diffusion. Ligands with a molecular weight over 500 will have difficulty penetrating the membrane, both in the skin and in the digestive tract, making them hard to absorb. The log P value reflects a compound's polarity. If log P > 5, the compound may have a higher potential for toxicity because it remains longer in the lipid bilayer, which reduces its binding selectivity to the target. The number of hydrogen bond donors and acceptors indicates that a higher capacity for hydrogen bonding requires more energy for absorption. Molar refraction, which refers to the molar size of a molecule, describes the steric properties of a compound that can affect compound-receptor interactions. The Calculated Molar Refraction (CMR) value, based on molar refraction, indicates that higher CMR values suggest more potent steric properties and less favorable interactions with the receptor [19,23,28,83]. In this study, the compounds identified by LC-ESI/MS in M. calabura fruit extract were then evaluated for their physicochemical properties and skin permeability (Figures 3a-3b).

The results of the physicochemical analysis of compounds based on Lipinski's rules showed that nine compounds (Figure 3a) did not me*et al*l five of Lipinski's criteria. These included Aloeresin A **(18)**, amaranthin **(19)**, Hispidulin 7-(6-E-p-coumaroyl-β-D-glucopyranoside) **(24)**, mahuannin A **(29)**, Nevadensin-5-O-β-D-glucoside **(34)**, Procyanidin B2 gallate **(38)**, Quercetin-3-O-glucuronide 6″-methylester **(40)**, and Quercetin-6-O-glucoside **(41)**. These compounds were considered to lack the ideal physicochemical properties mainly because of their high molecular weight or having more than 10 hydrogen acceptors, which requires more energy for absorption into the target. This tendency suggests that oral administration would be challenging for these compounds [28,84]. However, they could be suitable for topical or transdermal routes, as supported by skin permeability data shown in Figure 3b. The relationship between physical and chemical properties and skin permeability in Figure 3b indicates that most compounds possess favorable characteristics, although two compounds—2,5-Dimethyl-1,4-benzoquinone **(2)**, and Bavachromene **(20)**—are considered not to meet these criteria.

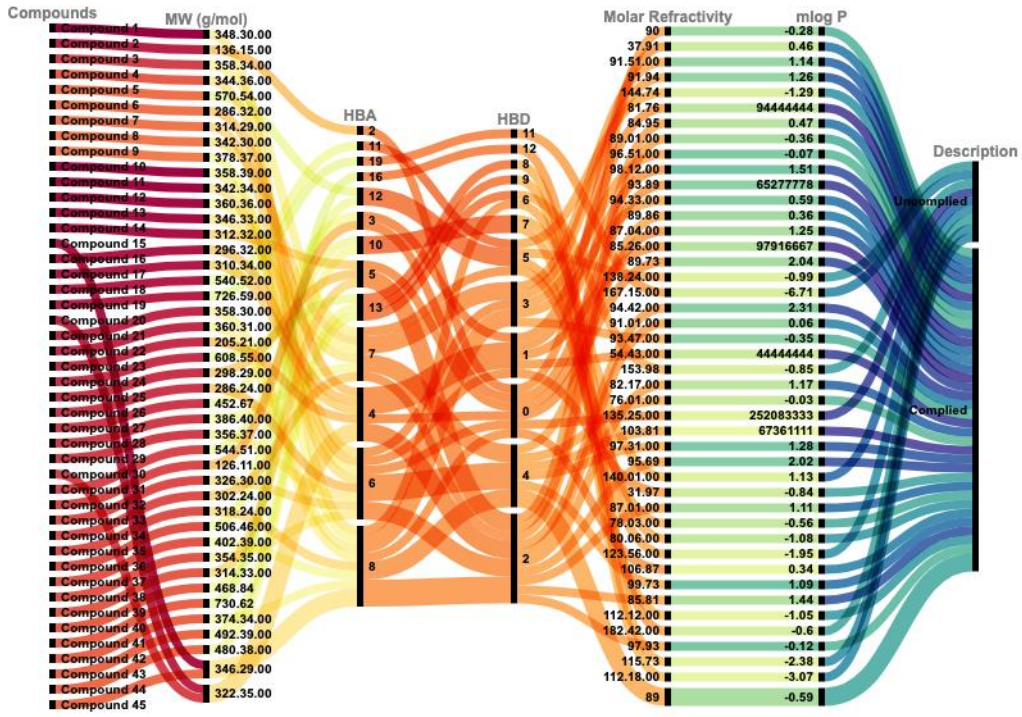

(a)

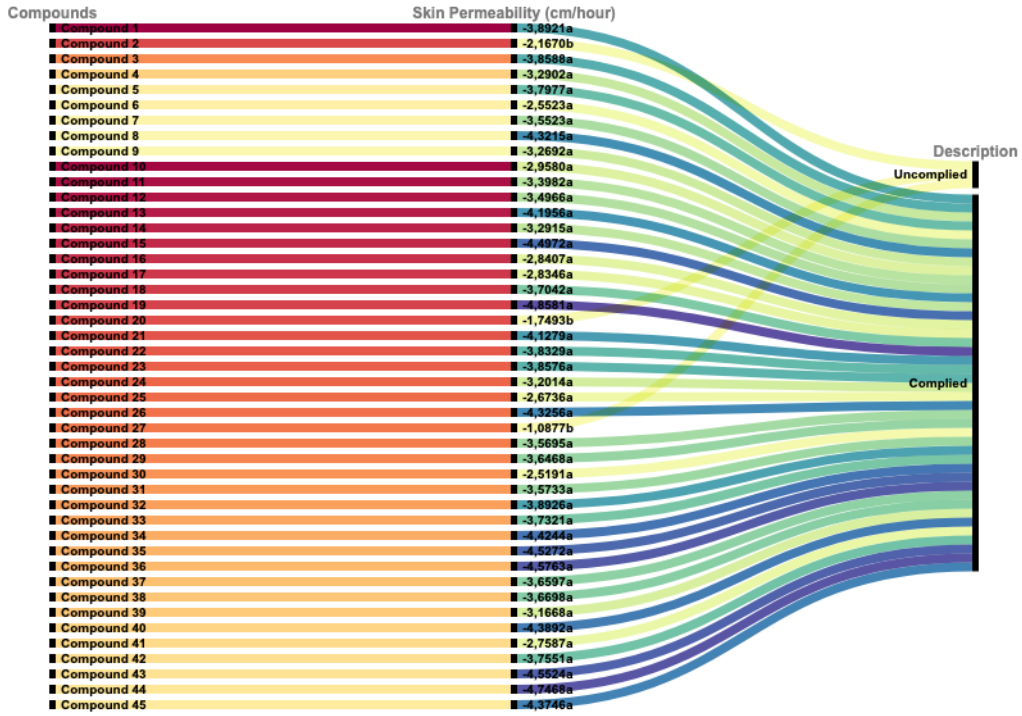

(b)

Figure 3. The physicochemical properties of **(a)** Lipinski Rule parameter; **(b)** skin permeability profiles of the compounds identified from *M. calabura* fruit extract were visualized using an alluvial diagram to assess the suitability of their parameters.

The compound's ability to penetrate the skin through topical administration results in a skin permeability score of > -2.5, indicating low skin permeability. The skin permeability parameter helps predict how well active substances are absorbed through the skin when applied topically. This prediction is based on the compound's ability to penetrate the skin barrier.

Compounds with ideal physical and chemical properties often show high permeability [5,21,85].

3.3. Network pharmacology-related antiaging analysis.

Network pharmacology offers a powerful approach for integrating predictive and genomic data to uncover the complex mechanisms underlying skin aging. By combining SwissTarget Prediction with GeneCards, a comprehensive framework was established to explore the molecular links between *M. calabura* metabolites and aging-related pathways. The integration of SwissTargetPrediction with GeneCards provided a robust framework for identifying molecular associations relevant to skin aging. From SwissTargetPrediction, 50 potential target proteins of Muntingia calabura secondary metabolites were identified, while GeneCards yielded 162 proteins annotated with the keyword "skin aging." The overlap between these datasets revealed 21 common proteins, which represent the critical intersection between phytochemical activity and aging-related molecular pathways. This convergence, visualized through a Venn diagram, highlights the subset of targets most likely to mediate the anti-aging potential of *M. calabura* (Figure 4a). The shared proteins suggest that bioactive metabolites from this plant may exert regulatory effects on pathways central to cellular senescence, oxidative stress, extracellular matrix remodeling, and inflammatory responses—mechanisms widely implicated in skin aging.

By narrowing the focus to these 21 interconnected targets, the network pharmacology approach provides a more precise map of how natural compounds may influence complex biological processes. This not only strengthens the rationale for further mechanistic studies but also underscores the translational relevance of *M. calabura* metabolites in developing novel interventions for age-related skin deterioration.

The screening of active compounds from *M. calabura* fruit identified 41 compounds related to molecules and genes (light blue nodes) associated with various diseases (dark blue nodes) (Figure 4b and 4c). Of these 41 compounds, data showed that 19 play a direct role in anti-aging mechanisms through interactions with 21 target genes (light blue nodes). In Figure 4a, *M. calabura* fruit extract is depicted as a red node on the left, connected to several active compounds, which are shown as deep green triangular nodes. Key compounds involved in anti-aging effects include 2,5-dimethyl-1,4-benzoquinone **(2)**, 2''-O-feruloylaloesin **(5)**, 2'-hydroxy-4', 6'-dimethoxy dihydrochalcone **(6)**, 2',7-dihydroxy-4',5'-dimethoxyisoflavone **(7)**, 4',5,6,7-tetramethoxy-flavone **(11)**, 5,7-dihydroxy-6-methoxyl-8-methyl-3-(2′,4′-dihydroxybenzyl) chroman-4-one **(13)**, 6-hydroxy-7-methoxy-2-(2-phenylethyl) chromone **(16)**, 6-methoxy-2-[2-(3'-methoxyphenyl) ethyl] chromone (17), aloeresin A **(18)**, bavachromene **(20)**, dichotomitin **(21)**, hispidulin 7-(6-E-p-coumaroyl-β-D-glucopyranoside) **(24)**, mahuannin A **(29)**, maltol **(30)**, morin **(32)**, nevadensin-5-O-β-D-glucoside **(34)**, procyanidin B2 gallate **(38)**, and quercetin-6-O-glucoside **(41)**. These compounds demonstrate pharmacological potential in slowing the aging process via various molecular mechanisms. Their interactions with target genes, represented by light blue hexagonal nodes, include IL-2, JAK2, TNF, MAPK14, MMP, and TYR (Figure 4b). These genes participate in biological processes such as inflammation, oxidative stress regulation, and tissue repair, collectively contributing to the anti-aging effects [81,86].

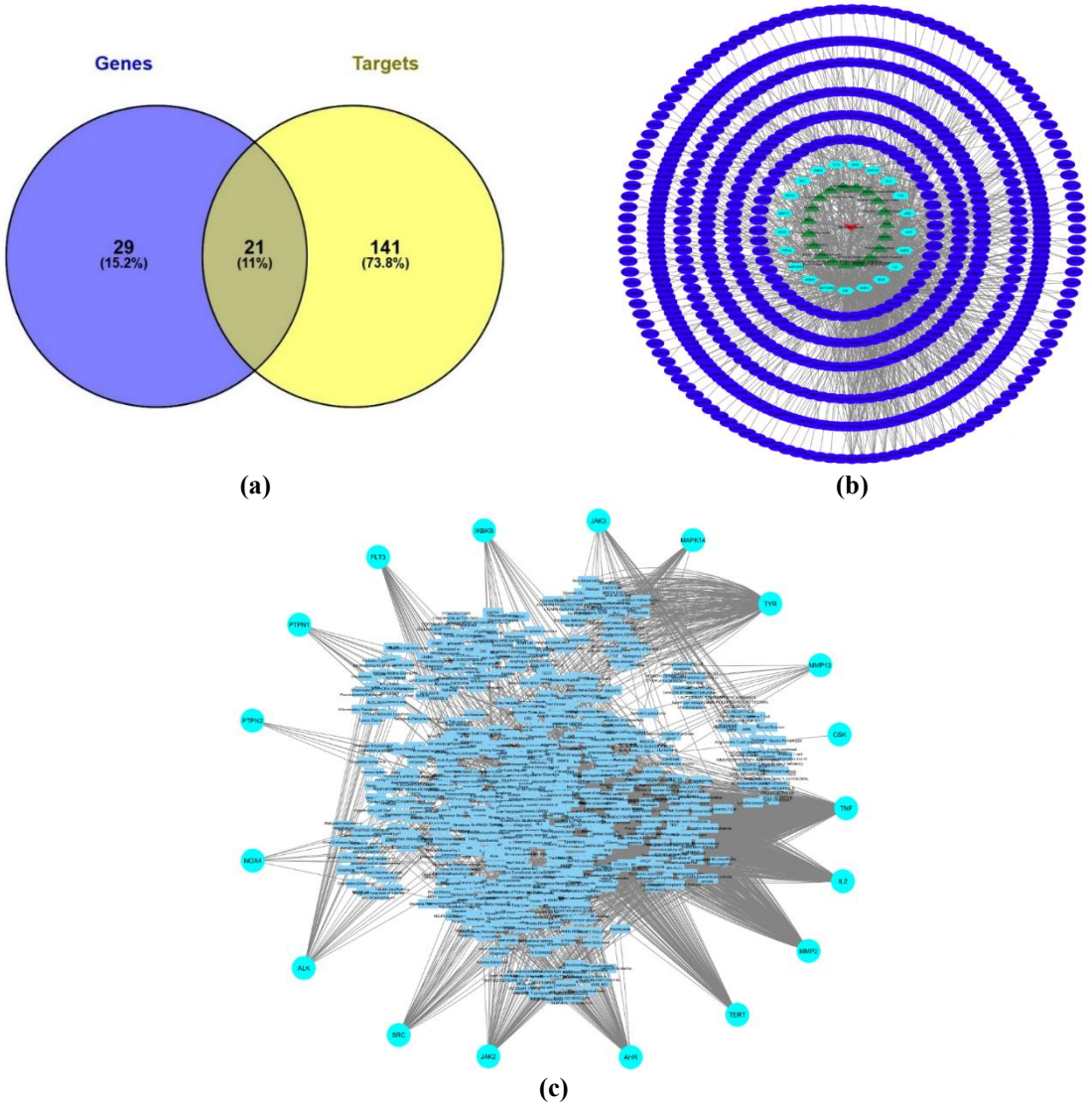

Figure 4. (a) Venn diagram illustrating the overlap between predicted target proteins of secondary metabolites from *Muntingia calabura* (SwissTargetPrediction) and genes associated with skin aging (GeneCards); **(b)** The visualization illustrates how multiple compounds from *M. calabura* fruit extract interact with various genes, pathways, and diseases through a pharmacological networking diagram. **Red nodes** (inverted triangles) represent the *M. calabura* fruit extract, **deep green nodes** indicate its molecular compounds, **light blue nodes** correspond to target genes or proteins, and **dark blue nodes** denote associated diseases; **(c)** A magnified view highlights the relationships between proteins targeted by *M. calabura* (**light blue nodes**) compounds and their corresponding diseases (**sky blue nodes**) (enlargement of Figure 4b).

Furthermore, these target genes interact with various biological pathways, as shown by the dark blue oval nodes on the right side of the network (Figure 4b). These pathways suggest that the anti-aging mechanism of compounds in *M. calabura* involves multiple processes, including modulation of inflammation, inhibition of oxidative stress, and enhancement of proteolytic and regenerative enzyme activity. This interaction pattern supports the concept of multi-target network pharmacology, which indicates that the pharmacological effects of this fruit do not rely on a single pathway but involve multiple interconnected molecular targets within a complex biological system [25]. The network pharmacology analysis in Figures 4b and 4c suggests that the bioactive compounds in *M. calabura* have strong potential for development as herbal-based anti-aging agents. However, to verify these interactions and better understand the molecular mechanisms involved, further studies, such as in vitro and in vivo experimental validation, are necessary. The results of this study also provide a scientific basis

for developing products based on active compounds from *M. calabura* as natural agents to prevent and slow the aging process.

Several compounds specifically bind target proteins that modulate premature aging, including those related to MAPK and pro-inflammatory genes. MAPK genes influence the increased production of skin-degrading enzymes in the extracellular matrix, such as MMPs and elastase (Figure 4c, light blue nodes). Meanwhile, other pro-inflammatory genes, including IL and TNF-α, activate tyrosinase in the EDN-1 pathway by increasing c-kit mRNA and downregulating collagen and elastin through the pro-inflammatory cytokine pathway [3]. These 21 target genes are involved in causing the premature aging process (Figure 4c). Further analysis in the network pharmacology evaluation revealed that compounds **(7)**, **(21)**, **(30)**, and **(32)** have significant interactions with the target gene Tyrosinase (TYR) ($p < 0.05$). The same occurs with compounds **(24)** and **(32)**, which directly link to the AHR gene, ultimately leading to increased tyrosinase induction. Additionally, compounds **18**, **29**, and **38** show significant interactions with MMP genes ($p < 0.05$). MMP genes, such as MMP-1, MMP-2, MMP-9, and MMP-13, encode matrix metalloproteinase enzymes that degrade collagen, elastin, and gelatin in skin tissue [35,87,88]. The activity of these enzymes increases with age, causing damage to the skin's structure and the development of wrinkles. Other compounds like **(2)**, **(5)**, **(6)**, **(11)**, **(13)**, **(16)**, **(17)**, **(20)**, **(34)**, **(38)**, and **(41)** target genes such as MAPK, IL-1, and TNF-α, which ultimately contribute to increased production of skin-degrading enzymes in MMPs and activation of tyrosinase (TYR). These compounds play a crucial role in anti-aging effects due to their influence on regulating skin pigmentation and extracellular matrix degradation. Tyrosinase (TYR) is a key enzyme in melanin biosynthesis, playing a crucial role in regulating skin pigmentation. Inhibiting this enzyme can reduce hyperpigmentation and prevent skin aging caused by oxidative stress. The interaction of compounds **(7)**, **(21)**, **(24)**, **(30)**, and **(32)** with TYR suggests that these compounds may help prevent excessive hyperpigmentation, supporting skin-lightening effects and protection against free radical-induced aging [89].

Several studies have clarified the molecular mechanisms through which compounds like maltol **(30)** show significant antioxidant and anti-inflammatory effects. This compound can decrease oxidative stress and inhibit the secretion of nitric oxide (NO) and key inflammatory cytokines, including interleukin (IL)-1β, IL-6, and tumor necrosis factor-α (TNF-α) [89]. Other compounds, such as Procyanidin B2 gallate **(38)**, are known to suppress MMP9 expression, which is involved in protecting against extracellular matrix breakdown and slowing skin aging. The mechanism of action of Procyanidin B2 gallate also involves the regulation of several important molecular pathways, including NF-κB, MAPK, PI3K/Akt, the apoptotic pathway, and Nrf2/HO-1, which are crucial in defending cells against oxidative stress and inflammation. These findings corroborate the notion that maltol and Procyanidin B2 gallate are two principal compounds that substantially contribute to the anti-aging effects of M. calabura, as evidenced by an in vitro study reported previously[89]. This evidence supports the idea that the pharmacological mechanisms of this plant can be harnessed for developing herbal-based anti-aging products, especially for preventing hyperpigmentation and maintaining skin elasticity.

The interpretation of this network pharmacology analysis indicates that the bioactive compounds in *M. calabura* have significant potential to be developed as herbal-based anti-aging agents. However, additional studies are necessary to confirm these interactions and better understand the molecular mechanisms involved, including in silico validation and in vitro and in vivo experiments. In this exploratory study, network pharmacology data were further

analyzed for potential molecular interactions using molecular docking. These results can serve as a scientific foundation for developing products based on active compounds from *M. calabura* as natural therapies to prevent and reduce the aging process.

3.4. Molecular docking analysis.

The outcomes of the pharmacological network analysis, represented by potential compounds associated with aging-related target genes, demonstrate that the MMP and TYR genes are the principal genes exhibiting the highest centrality values. These genes actively influence the increased activation of skin tissue-degrading enzymes, including collagenase, gelatinase, elastase, and tyrosinase. These four enzymes served as target proteins to investigate their molecular interaction mechanisms via a docking approach. The following list includes the target proteins used in the molecular docking study, which have been confirmed by previous docking validated analyses against native ligands (Table 3).

Molecular docking simulations were carried out using AutoDock 4.2, applying the Lamarckian Genetic Algorithm (LGA) as the search method. To ensure reproducibility and accuracy, the docking parameters were carefully defined. Each ligand was subjected to 50 independent GA runs, with a population size of 150 individuals per run. The algorithm was allowed to perform up to 2.5×10^6 energy evaluations and a maximum of 27,000 generations before termination. The mutation rate was set at 0.02, while the crossover rate was maintained at 0.8, in accordance with standard AutoDock protocols. Step sizes for conformational sampling were specified as 0.2 Å for translational movements, 5° for quaternion rotations, and 5° for torsional degrees of freedom. These parameters were selected to balance computational efficiency with reliable exploration of the conformational space, thereby providing robust predictions of ligand–protein binding interactions [90].

Validation was carried out by re-docking each native ligand molecule of collagenase and gelatinase to the active site of its receptor using the grid box and coordinates specified in Table 3. These coordinates include the amino acid residues involved in ligand binding, allowing a comparison between the native ligand's position and the re-docked ligand (re-docking results). The validity of the docking method was assessed based on the Root Mean Square Deviation (RMSD) value, with an RMSD of less than 2 Å indicating results close to experimental data. The validation results showed an RMSD value of less than 2 Å for each natural ligand, thus meeting the criteria. The smaller the RMSD, the closer the re-docked ligand's position is to the crystallographic ligand [3,23,26].

Table 3. *gridbox* and RMSD values from the validation results of the docking method.

Protein	Gridbox	Coordinat (x,y,z)	RMSD (Å)	Visualization of Protein	Visualization of native ligands and copy ligands
Collagenase (PDB ID: 2D1N)	22×33×43	-44.320 25.911 -19.703	1.899	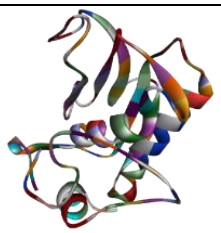 Chain A	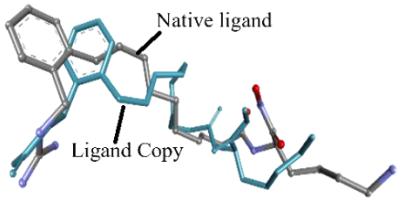

Protein	Gridbox	Coordinat (x,y,z)	RMSD (Å)	Visualization of Protein	Visualization of native ligands and copy ligands
Gelatinase (PDB ID: 1GKC)	40×40×40	65.607 31.083 117.843	1.081	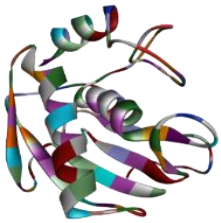 Chain A	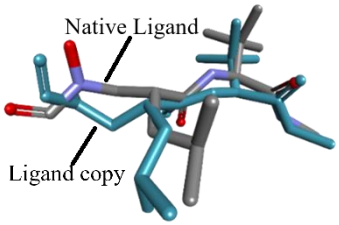
Elastase (PDB ID: 3HGN)	40×40×40	12.871 9.278 2.197	1.34	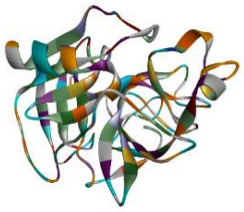 Chain A	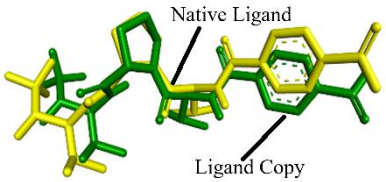
Tyrosinase (PDB ID: 5M8L)	16×12×18	25,911 104,236 154,966	1.486	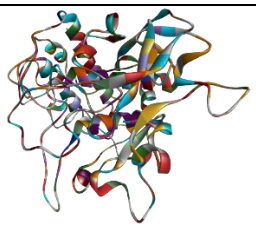 Chain C	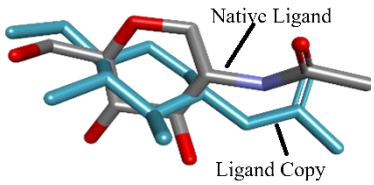

Based on the results of the previous pharmacology network analysis, 19 potential compound candidates were identified from *M. calabura* fruit extract, as they relate to target genes and proteins that contribute to skin aging. The 19 target compounds were assessed for their interactions with MMP proteins, including collagenase, gelatinase, elastase, and gen Tyr, including tyrosinase. The evaluation generally showed interactions with the target proteins; however, among the 19 compounds, three main compounds were selected for their optimal interactions with the target proteins, based on their binding free energy values and hydrogen and van der Waals interactions with the amino acid residues of the target proteins (Table 4). A more negative free energy value indicates a spontaneous and stable interaction between the compound and the target protein [11,23,28]. The free binding energy reflects the stability of the ligand when bound to its target; the more negative the value, the more stable the interaction [91]. These results suggest that the tested compounds can form stable interactions with target proteins, potentially exerting anti-aging effects.

Table 4. The binding affinity and hydrogen/van der Waals interaction between compounds identified and the protein target.

Compound Code	Molecule Name	Collagenase (2D1N)		Gelatinase (1GKC)		Elastase (3HGN)		Tyrosinase (5M8L)	
		Binding affinity (kcal/mol)	H-Bond/Van der Waals Interaction	Binding affinity (kcal/mol)	H-Bond/Van der Waals Interaction	Binding affinity (kcal/mol)	H-Bond/Van der Waals Interaction	Binding affinity (kcal/mol)	H-Bond/Van der Waals Interaction
	Native ligand	-7.16	PRO236, ALA238, HIS222, HIS232, LEU185, ALA238, ALA186, ILE243, THR245	-7.56	LEU188, TYR423, GLU402, LEU187, MET422	-7.71	VAL216, HIS57, GLY193, SER195, ARG217A, GLN192, PHE215	-2.53	ASN318, ALA320, ASN385, GLY317
2	2,5-Dimethyl-1,4-benzoquinone	-5.31	-	-5.74	-	-5.17	GLY193, SER195,	-2.72	ALA320, ASN385

Compound Code	Molecule Name	Collagenase (2D1N)		Gelatinase (1GKC)		Elastase (3HGN)		Tyrosinase (5M8L)	
		Binding affinity (kcal/mol)	H-Bond/Van der Waals Interaction	Binding affinity (kcal/mol)	H-Bond/Van der Waals Interaction	Binding affinity (kcal/mol)	H-Bond/Van der Waals Interaction	Binding affinity (kcal/mol)	H-Bond/Van der Waals Interaction
							VAL216, PHE215		
5	2"-O-Feruloylaloesin	-6.14	HIS232,	-9.00	TYR423	-7.53	VAL216, ARG217A, PHE215,	0	-
6	2′-Hydroxy-4′,6′-dimethoxydihydrochalcone	-8.57		-8.24	GLU402	-6.22	HIS57, SER195 VAL216	-1.03	ASN318, ASN385
7	2′,7-Dihydroxy-4′,5′-dimethoxyisoflavone	-9.17	ILE243, THR245,	-7.01	GLU402	-6.59	VAL216, SER195, GLY193, ARG217A,	0	-
11	4',5,6,7-Tetramethoxy-flavone	-9.07	LEU185, HIS222, THR245	-7.57	-	-6.45	GLN192, GLY193, SER195, VAL216	0	-
13	5,7-Dihydroxy-6-methoxyl-8-methyl-3-(2′,4′-dihydroxybenzyl) chroman-4-one	-7.62	-	-7.51	LEU188, TYR423, LEU187	-7.08	SER195, VAL216, GLY193, GLN192	0	-
16	6-Hydroxy-7-methoxy-2-(2-phenylethyl) chromone	-8.65	LEU185, HIS232, ILE243	-8.91	GLU402, LEU187, MET422	-7.26	SER195, VAL216, GLN192	-1.31	ASN318, ASN385, ALA320
17	6-Methoxy-2-[2-(3'-methoxyphenyl) ethyl] chromone	-9.19	PRO236, ALA238, HIS222	-8.70	-	-6.66	GLN192, SER195, VAL216	-0.68	GLY386, ASN385
18	Aloeresin A	-9.65	LEU185, ALA186, HIS222	-11.40	GLU402, LEU187	-8.58	VAL216, GLN192, SER195	0	-
20	Bavachromene	-10.50	ALA238, ILE243	-10.89	GLU402	-8.48	VAL216, SER195	0	-
21	Dichotomitin	-9.60	ILE243, THR245	-7.82	GLU402	-6.44	VAL216, GLY193, GLN192, PHE215	0	-
24	Hispidulin 7-(6-E-p-coumaroyl-β-D-glucopyranoside)	-6.39	LEU185	-9.39	LEU188, LEU187	-6.62	ARG217A, PHE215	0	-
29	Mahuannin A	0	THR245	-7.87	MET422, GLU402, TYR423	-7.26	VAL216, ARG217A, PHE215, SER195	0	-
30	Maltol	-4.89	ILE243	-5.08	MET422	-4.85	GLY193, SER195, GLN192	-2.62	GLY317, ALA320, ASN385
32	Morin	-7.28	HIS222, HIS232, LEU185	-7.44	GLU402	-6.81	SER195, GLY193, VAL216, GLN192, PHE215	0	-
36	Nevadensin-5-O-β-D-glucoside	-8.42	-	-7.68	LEU188, TYR423, GLU402, LEU187,	-6.39	GLN192, SER195, ARG217A, VAL216	0	-
38	Procyanidin B2 gallate	0	ILE243	-6.64	MET422,	-5.75	SER195, VAL216,	0	-

Compound Code	Molecule Name	Collagenase (2D1N)		Gelatinase (1GKC)		Elastase (3HGN)		Tyrosinase (5M8L)	
		Binding affinity (kcal/mol)	H-Bond/Van der Waals Interaction	Binding affinity (kcal/mol)	H-Bond/Van der Waals Interaction	Binding affinity (kcal/mol)	H-Bond/Van der Waals Interaction	Binding affinity (kcal/mol)	H-Bond/Van der Waals Interaction
							ARG217A, PHE215		
41	Quercetin-6-O-glucoside	-7.27	HIS232	-5.05	LEU188	-5.18	VAL216, PHE215	0	-

The three compounds include: Compounds **(18)**, **(20)**, and **(21)** which are optimal for collagenase protein; compounds **(18)**, **(20)**, and **(24)** for gelatinase protein; compounds **(16)**, **(18)**, and **(20)** show the best interaction with elastase protein; and compounds **(2)**, **(16)**, and **(30)** are the top performers in interacting with tyrosinase protein (Figures 5a-5d). Each of these three selected compounds has a more negative binding free energy (kcal/mol) and tends to be close to or even more negative than its native ligand. Additionally, the three compounds are supported by their interactions with target proteins that resemble the native ligand for each target (Table 4). Further observation revealed that compounds 6-Hydroxy-7-methoxy-2-(2-phenylethyl) chromone **(16)**, Aloeresin A **(18)**, and Bavachromene **(20)** interacted very well with MMPs target proteins, specifically collagenase (-8.65, -9.65, and -10.50 kcal/mol), gelatinase (-8.91, -11.40, and -10.89 kcal/mol), and elastase (-7.26, -8.58, and -8.48 kcal/mol), respectively.

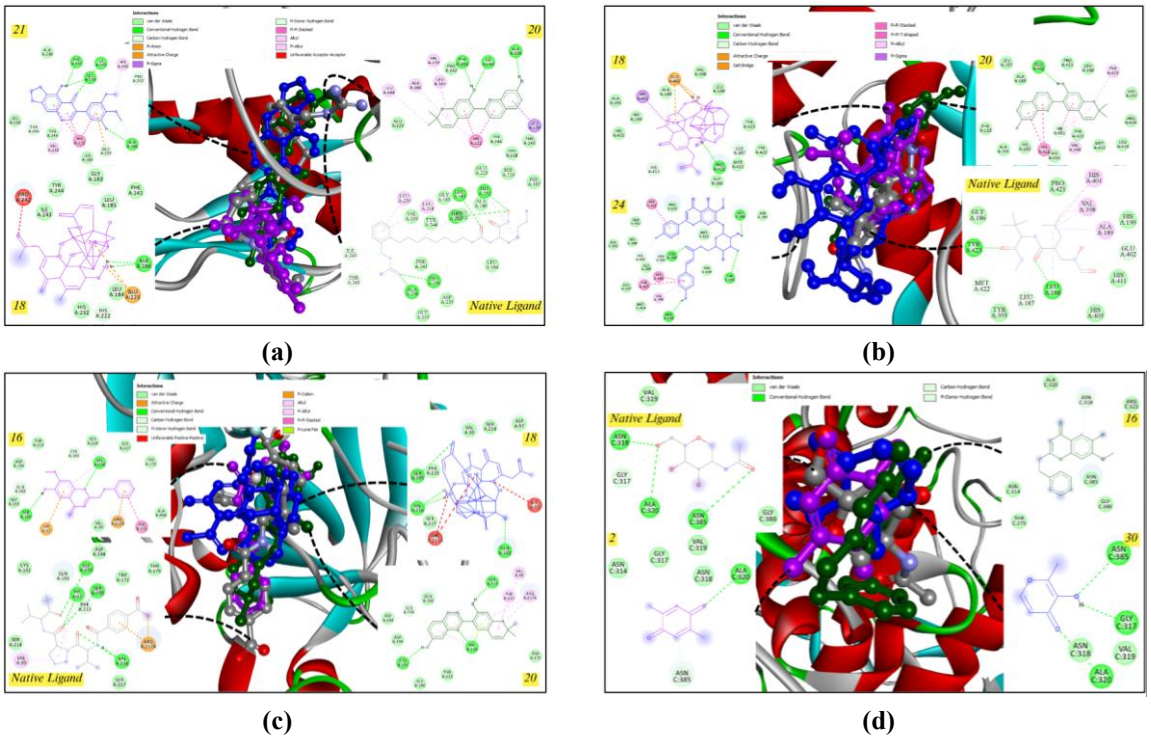

(a) **(b)** **(c)** **(d)**

Figure 5. Visualisation of the interaction results between the most active molecules on **(a)** collagenase; **(b)** gelatinase; **(c)** elastase; **(d)** tyrosinase proteins. Three selected compounds interacted with each of the target proteins. The visualisation shows that the three most active compounds can inhibit each enzyme with a mechanism almost identical to that of the target protein. The inhibitory interaction of the most active compounds occurs on amino acids similar to the native ligand. The native ligand of protein target are N-[(2R)-6-amino-1-(hydroxyamino)-1-oxo-hexan-2-yl]-10-[2-(carbamimidamidomethyl)phenyl]-decanamide (collagenase), N~2~-[(2R)-2-{[formyl(hydroxy)amino]methyl}-4-methylpentanoyl]-N,3-dimethyl-L-valinamide (gelatinase), 4-[[(2S)-3-methyl-1-oxo-1-[(2S)-2-[[(3S)-1,1,1-trifluoro-4-methyl-2-oxo-pentan-3-yl]carbamoyl]pyrrolidin-1-yl]butan-2-yl]carbamoyl]benzoic acid (elastase) and 2-acetamido-2-deoxy-beta-D-glucopyranose (tyrosinase).

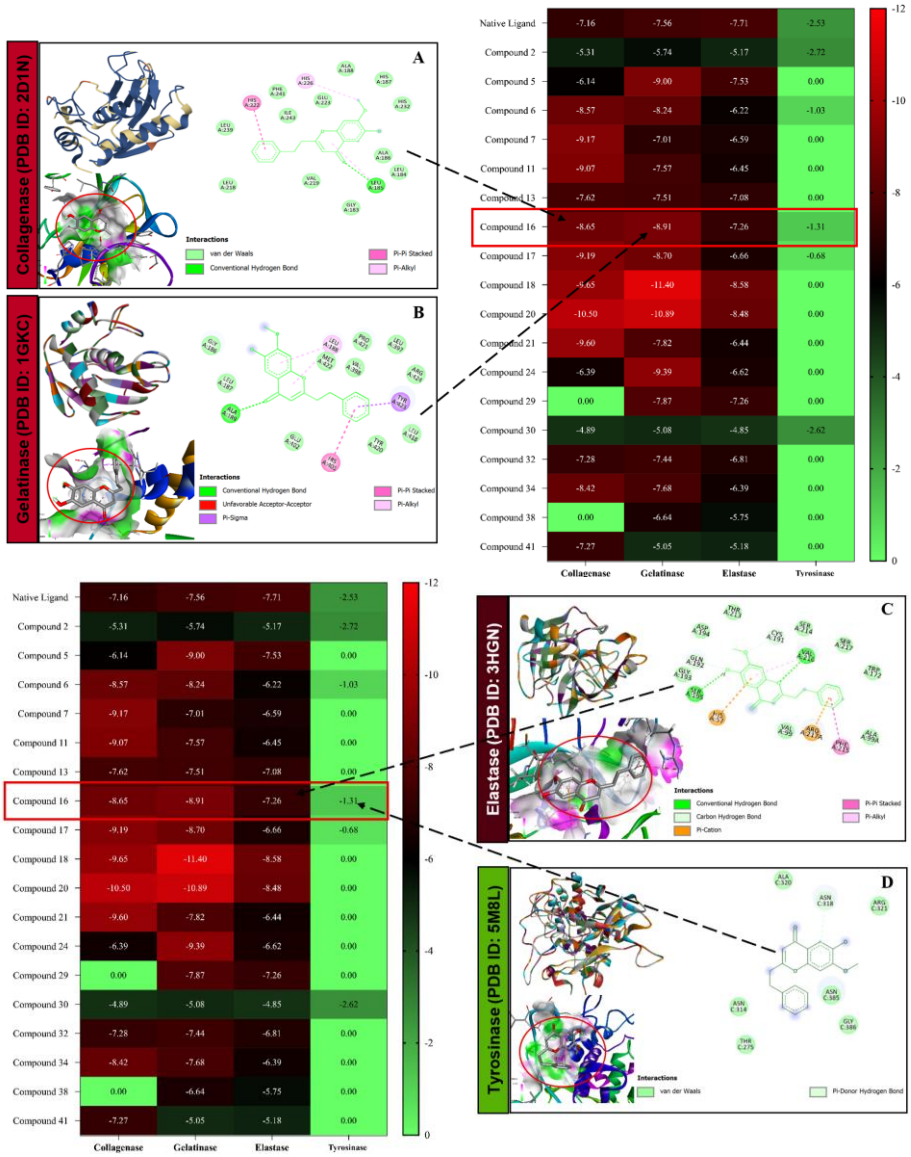

Figure 6. A comparison of the binding affinity values of each identified compound, which has an antiaging mechanism of action through inhibition of collagenase, gelatinase, elastase, and tyrosinase, was presented using heatmap analysis. Potential compounds that target multiple sites related to the ageing mechanism were selected for subsequent analysis of their interaction patterns with **(a)** collagenase; **(b)** gelatinase; **(c)** elastase; **(d)** tyrosinase.

Compounds (**16**), (**18**), and (**20**), which show potential against MMPs target proteins, are derivatives of the flavonoid group. Their chemical structures suggest that the hydroxyl (-OH) and carbonyl (C=O) groups in flavonoids facilitate the formation of hydrogen or Van der Waals bonds with collagenase, gelatinase, and elastase proteins. Amino acid residues such as LEU185, HIS232, HIS222, Ile243, Ala186, and Ala238 in collagenase tend to interact with the hydrogen atoms on the -OH and C=O groups of compounds in *M. calabura* fruit extract. In gelatinase, hydrogen interactions occur at amino acids Glu402, Leu187, and Met422, while in elastase proteins, hydrogen bonds form with the -OH and C=O groups of amino acid residues Ser195, Val216, and Gln192 (Table 4 and Figure 5). These amino acids are the active sites where the native ligand interacts with the protein. Therefore, it is reasonable to conclude that the active compounds from *M. calabura* fruit extract could provide equal or even better inhibition than the native ligand. Unfortunately, compounds 18 and 20 did not inhibit the target protein tyrosinase, as indicated by an undetermined binding free energy value (0) (Figure 5). However, compound 16 showed inhibitory activity, with a binding free energy of -1.31

kcal/mol, although this is lower than the binding free energy of the native ligand at -2.53 kcal/mol.

Based on the heatmap analysis (Figure 6), only compound (16) inhibits all targets associated with premature aging. The binding free energy values of compound **(16)** against the target proteins collagenase, gelatinase, elastase, and tyrosinase are -8.65, -8.91, -7.26, and -1.31 kcal/mol, respectively. The binding free energy of the *M. calabura* compound against each target is similar to or even higher than the native ligand's binding free energy: -7.16 kcal/mol for collagenase, -7.56 kcal/mol for gelatinase, -7.71 kcal/mol for elastase, and -2.53 kcal/mol for tyrosinase. Additionally, analyzing the interaction pattern of the compound from *M. calabura* fruit extract suggests that compound **(16)** may have multi-target potential for inhibiting proteins involved in premature aging, such as collagenase, gelatinase, elastase, and tyrosinase. Compound **(16)** can be further developed as an anti-aging agent, as demonstrated directly by in vitro and in vivo methods. Additionally, compound (16) is predicted to exhibit relatively safe topical toxicity, as indicated by several parameters, including eye irritation, skin sensitization, and skin irritation. These predictions were generated using ADMETlab 3.0 (http://scbdd.com/) for eye irritation and skin sensitization, and admetSAR 3.0 (https://lmmd.ecust.edu.cn/admetsar3/resource.php) for skin irritation. The results, summarized in Table 5, provide an overview of the predicted topical toxicity profiles of the most active compounds against the target protein.

Table 5. Prediction of the topical exposure toxicity for each active compound in *M. calabura* fruit extract.

Comp. Code	Compound name	Eye irritation	Skin sensitization	Skin irritation
2	2,5-Dimethyl-1,4-benzoquinone	0.999	0.994	1
16	6-Hydroxy-7-methoxy-2-(2-phenylethyl) chromone	0.420	0.309	0
18	Aloeresin A	0.095	0.956	0
20	Bavachromene	0.962	0.901	1
21	Dichotomitin	0.914	0.325	0
24	Hispidulin 7-(6-E-p-coumaroyl-β-D-glucopyranoside)	0.641	0.987	0
30	Maltol	0.991	0.292	1

Skin irritation prediction aims to identify potential side effects in humans, while skin sensitization gauges the skin's sensitivity to chemicals that can cause allergies [92]. Evaluation of eye irritation (EI) potential is essential for assessing the risk of injury to the cornea and conjunctiva fromhemicals [24]. These three parameters are key factors in assessing the safety of a raw material that can be developed as an active cosmetic ingredient. Previous research reports indicate that the active compounds in cosmetic raw materials have a safety toxicity range of 0-0.3 for relatively safe levels, 0.3-0.7 for moderate exposure toxicity, and 0.7-1 for poor safety [24]. The toxicity evaluation results showed that compound **(16)** is relatively safer for use as a potential active cosmetic ingredient, especially as an anti-aging agent. However, this prediction requires further justification through in vitro and in silico approaches to ensure the study's sustainability for application as an anti-aging cosmetic.

3.5. Molecular dynamics analysis.

Compound 16, whose activity has been determined through molecular docking, exhibits multitarget interactions with MMP proteins, including collagenase, gelatinase, elastase, and other proteins like tyrosinase. Therefore, the interaction's stability was assessed using a molecular dynamics approach. The Internal Coordinates Standard Mode Analysis (iMOD)

server was utilized to evaluate the interaction characteristics of compound 16 with various target proteins, using several key parameters including root mean square fluctuation (RMSF), deformability against index atoms, B-factor against index atoms, index residue matrix, eigenvalue against index mode, and percentage of variance against index mode [29,30,93]. The iMOD server enables the understanding of the flexibility and collective motion of macromolecules, such as proteins and amino acids, in response to various compounds. This analysis model is an efficient alternative to full-atomistic molecular dynamics (MD) simulations, especially for large biological molecule systems [31].

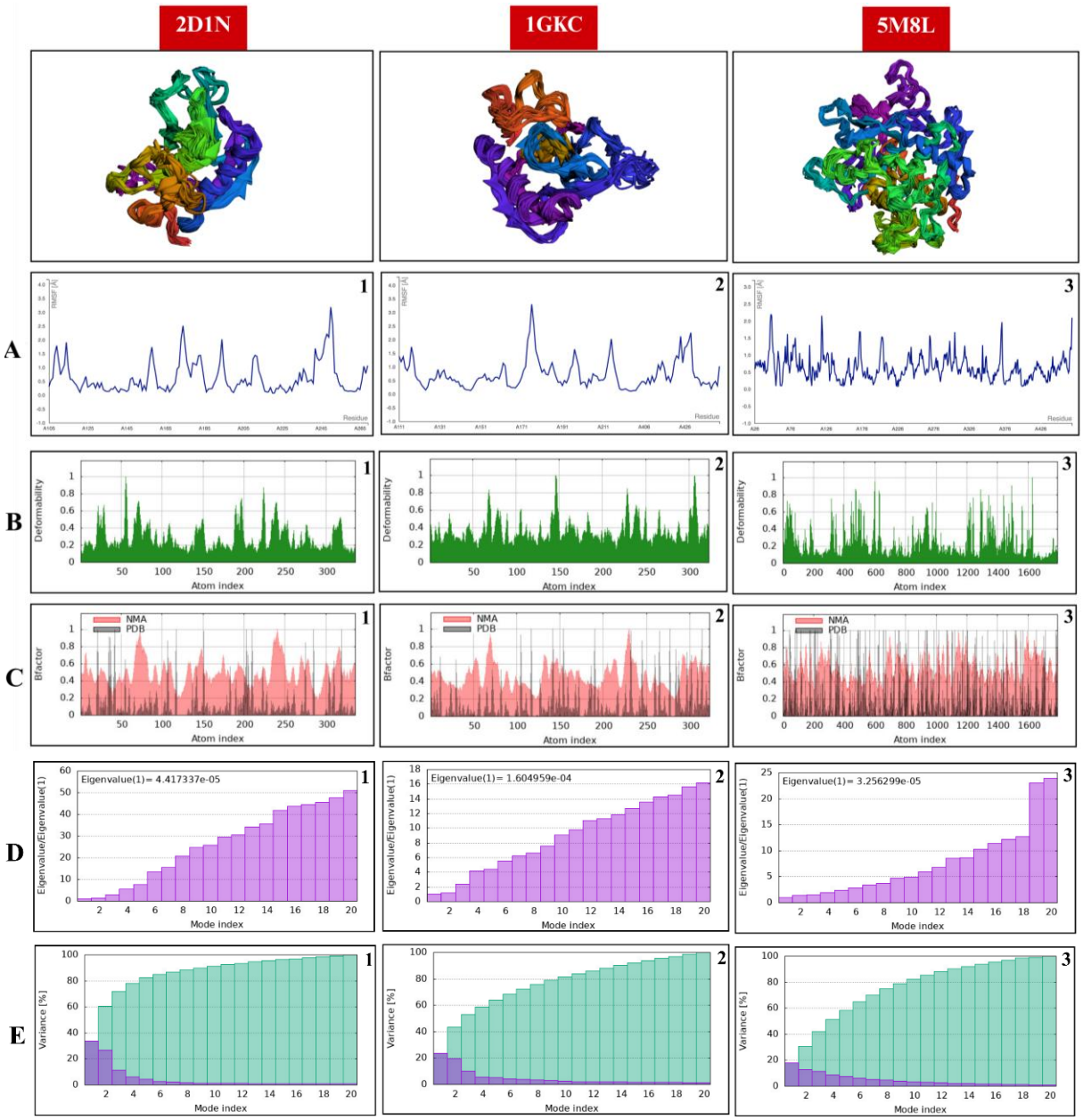

Figure 7. iMOD analysis of compound 16 against various proteins: 2D1N (collagenase), 1GKC (gelatinase), and 5M8L (tyrosinase). **(A)** Root mean square fluctuation (RMSF) values; **(B)** representation of the potential deformability graph of residue interactions; **(C)** B-factor relationship profile against index atoms; **(D)** eigenvalue profile over mode index; **(E)** percentage variation over mode index for each protein target of compound 16.

In the molecular dynamics analysis performed using the iMODS server, the residues considered correspond to the amino acid sequence of each target protein chain selected for docking (Collagenase: Chain A of PDB ID 2D1N, Gelatinase: Chain A of PDB ID 1GKC,

Elastase: Chain A of PDB ID 3HGN, and Tyrosinase: Chain C of PDB ID 5M8L). The total number of residues included in the simulation was 249 for collagenase, 388 for gelatinase, 240 for elastase, and 529 for tyrosinase, respectively. Residues were determined directly from the crystallographic structures deposited in the RCSB Protein Data Bank, after removal of water molecules, ions, and non-essential ligands during receptor preparation. The results of the molecular dynamics analysis are presented in Figure 7a-7e.

Molecular dynamics simulation results indicated that compound 16 maintained consistently low RMSF values and stable deformability indices throughout the simulation. These parameters confirm that the ligand–protein complex remained structurally stable, suggesting a strong and sustained interaction. Such stability supports the biological relevance of compound 16, as it is capable of effectively maintaining its inhibitory effect on the target protein over time (Figure 7a). Overall, the 2D1N and 1GKC proteins indicate that residues 10-100 exhibit low RMSF values, suggesting that the proteins bind to compound 16 with a stable interaction [31,94]. This demonstrates that the compound is firmly bound to this area, with fluctuations occurring only at residues 100-110. The residues around 100-110 show high RMSF values, which then decrease again, possibly due to the partial closure of the loop by compound 16 during interaction. High RMSF peaks in regions far from the 2D1N and 1GKC protein-binding sites likely indicate involvement in allosteric dynamics or ligand-access pathways. This may be necessary for the interaction of compound 16 with the protein to demonstrate the flexibility required for protein function or to accommodate the ligand, ensuring it does not appear rigid [31]. However, when compared to the 5M8L protein, it shows a slightly different fluctuation profile. Protein stability was observed at residues 10-30, indicating that the binding process of compound 16 had just begun and resulted in tight binding and constant fluctuations that started at residues 30-50 and continued to the furthest residue region with RMSF values ranging from 1.5 to 2.0, suggesting the possibility of partial closure of the protein loop by compound 16 during interaction. Notably, this fluctuation still occurs at a low RMSF value compared to the 2D1N and 1GKC proteins, indicating that the interaction remains regular and stable [30].

Analysis using the iMOD server also provided deformability profiles and B-factors for the main chain, as well as the deformation properties of each residue. Figures 7b and 7c display the deformability and B-factor of each protein. The deformability profiles show relatively high peaks, indicating significant deformation in both the 2D1N, 1GKC, and 5M8L proteins. Higher peaks in the deformability graph suggest greater deformation potential of the residue. Residues with high deformability values are often part of "hinges" or flexible regions within the structure [31,94]. This aligns with the B-factor matrix of each protein, as shown in Normal Mode Analysis (NMA), in Figure 7c. Overall, the protein exhibits low-frequency normal modes, meaning it is in its minimum-energy state (pink), allowing it to vibrate or fluctuate around its equilibrium position. With low energy, the protein can be activated, facilitating effective interactions [31]. The low-frequency normal mode is also reflected in the relatively low eigenvalues, as shown in Figure 7d. The eigenvalues for each protein-ligand interaction (compound 16) were recorded at 4.417337e-05, 1.604959e-04, and 3.256299e-05, respectively. The eigenvalue scale from the molecular dynamics analysis using the iMOD server indicates a low scale. The lowest eigenvalue corresponds to the interaction with the 1GKC protein, followed by 5M8L and 2D1N. The small eigenvalue depicted in Figures 7d and 7e corresponds to this low-frequency mode. The smaller the eigenvalue, the lower the frequency and the easier (energetically) it is to activate the mode, indicating greater interaction flexibility [31]. Overall,

this study demonstrates that the complex of compound 16 with the target proteins 1GKC, 5M8L, and 2D1N exhibits good and stable interaction deformation.

Dynamic molecular analysis via the iMOD server also generated the covariance matrix and correlation of the residue indices in compound 16 and the protein complex. Figure 8 illustrates the covariance matrix and correlation of the residue indices. The heatmap of the covariance matrix in Figure 8 shows that the positions of residues in the macromolecule tend to vary together. Each vertical ***(i)*** and horizontal (***j***) element in the matrix represents the covariance between the movements of residue ***i*** and residue ***j*** within each protein complex and compound [31,95]. In the covariance matrix, the prominent red color observed in the 5M8L (Figure 8c) protein complex, with only a few blue and white areas, indicates a positive correlation. This suggests that there is a movement in the same direction at residue index ***i*** and ***j*** within the compound complex [31,94,95].

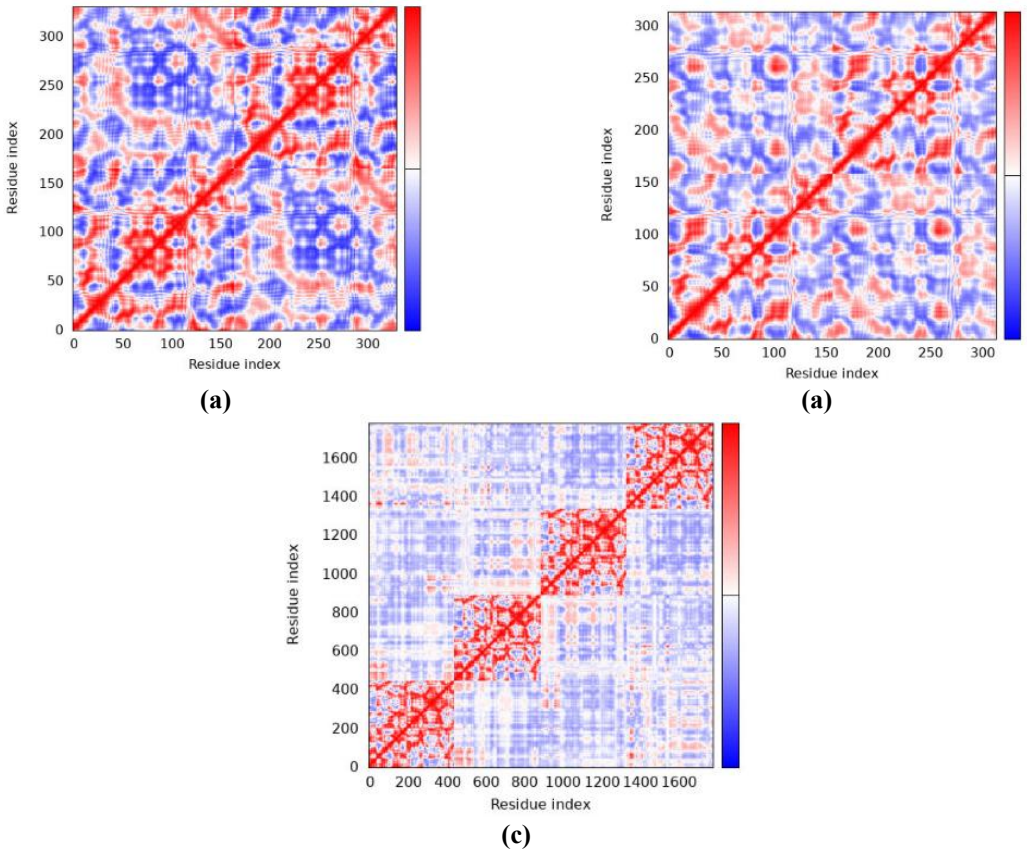

Figure 8. Heatmap of covariance and correlation matrix to residue index **(a)** protein complex of 1GKC; **(b)** protein complex of 2D1N; **(c)** protein complex of 5M8L. "In the iMODS visualization, the covariance matrix is presented as a heatmap. In this representation, red indicates a positive correlation, meaning residues tend to move in the same direction; blue indicates a negative correlation, meaning residues move in opposite directions; and white generally indicates no correlation or insignificant movement. This graphical output provides insight into the collective motions of residues within the protein structure, allowing identification of regions that move cooperatively or independently. Such information is crucial for understanding the dynamic stability of the ligand–protein complex, as highly correlated regions often contribute to structural rigidity, whereas negatively correlated or uncorrelated regions may reflect flexibility that influences binding stability and functional activity.

A similar phenomenon is observed in the 1GKC (Figure 8b) and 2D1N (Figure 8) protein complexes, where a dominant red area persists alongside noticeable blue and white regions, both of which still indicate positive covariance. A positive covariance matrix reflects a strong correlation between residues (***i*** and ***j***), which can be seen in the direction of molecular interactions (red linear regression profiles in each protein complex matrix). This matrix helps

identify regions in the molecule that move in a coordinated way, providing insights into the biological function or structural stability of the molecule under study [31]. Overall, the complex of compound 16 with the protein contains groups of residues that move together, potentially forming functional domains or playing roles in allosteric processes, thereby maintaining the stability of the complexed molecule.

The geometric interpretation of the plots in Figure 8 provides valuable insight into the dynamic behavior of residues within the three-dimensional protein structure. Peaks observed in the deformability and B-factor plots correspond to loop regions or surface-exposed residues, which are typically more flexible and prone to conformational changes. Conversely, troughs in these plots represent residues located within α-helices or β-sheets, reflecting the rigid core of the protein. The covariance matrix further highlights cooperative motions among residues: red regions indicate positively correlated movements, often within the same secondary structure elements, whereas blue regions denote negatively correlated motions, typically occurring between adjacent domains. These structural interpretations clarify why residues within the binding pocket (e.g., HIS232, GLU402, SER195) exhibit limited fluctuation, thereby contributing to the stabilization of ligand interactions. In contrast, flexible loop residues surrounding the active site introduce variability in the molecular dynamics outcomes, underscoring the interplay between structural rigidity and local flexibility in determining complex stability [96].

The molecular dynamics observation of the compound and protein 3HGN complex in this study could not be determined. Although molecular docking showed a strong interaction with negative binding affinity, it was impractical to evaluate the stability of the molecular interaction using the iMOS server approach. This is likely because the number of residues considered to provide interaction is minimal, making it impossible to assess the interaction's mobility with the iMOD server approach. This situation may be one of the limitations of using the iMOD server method. Nevertheless, iMODS remains an invaluable tool in protein dynamics analysis due to its speed and ease of use, especially for gaining an initial overview of biologically relevant collective motions [30,93]. The server provides quick assessments of stability parameters such as RMSF, deformability, and eigenvalues, but lacks detailed trajectory visualization and interaction mapping. For more comprehensive visualization and dynamic trajectory analysis, advanced platforms such as GROMACS may be employed. Future studies could therefore integrate GROMACS or similar MD packages to complement iMODS, providing both quantitative stability indices and visual confirmation of ligand–protein interactions [97,98]. Ultimately, more computationally intensive, full-scale MD simulations are required for accurate characterization, and the complex of compound 16 with protein 3HGN represents a promising candidate for further evaluation using these approaches.

4. Conclusions

In summary, 41 compounds from the ethanol extract of *Muntingia calabura* fruit were successfully identified using LC-ESI/MS. Pharmacologically, 19 of these compounds were directly associated with aging-related genes, including matrix metalloproteinases (MMPs) and tyrosinase. These compounds demonstrated strong interactions with key proteins, including collagenase, gelatinase, and elastase, and several also interacted with tyrosinase. Among them, 6-hydroxy-7-methoxy-2-(2-phenylethyl) chromone (compound 16), a homoisoflavonoid derivative, emerged as the most significant finding due to its multi-target potential. Compound 16 simultaneously inhibited collagenase, gelatinase, elastase, and tyrosinase, and molecular

dynamics studies confirmed the stability of these interactions, indicating that the compound can effectively maintain its inhibitory effects over time. This multi-target activity is particularly important, as complex aging mechanisms are often more effectively addressed by compounds that act on multiple pathways rather than single targets.

Looking ahead, while the present study provides strong in silico evidence, further in vitro and in vivo validation is essential to confirm the anti-aging potential of *M. calabura* fruit extract. Direct testing in cell culture systems and animal models will be critical for evaluating its biological efficacy, safety, and potential as a natural anti-aging agent. Such studies will not only substantiate the computational findings but also pave the way for translational applications in skincare and therapeutic formulations.

Author Contributions

Conceptualization, S.N. and F.J.S.; methodology, A.B.N., M., and A.B.; software, L.A.S., I., and D.M.W.; validation, N. and S.N.; formal analysis, A.B.N. and N.T.; investigation, A.B.N.; resources, S.N.; data curation, A.B. and L.A.S.; writing—original draft preparation, S.N. and A.B.N.; writing—review and editing, N. and N.T.; visualization, A.B., D.M.W., and I.; supervision, S.N.; project administration, M. and A.B.N.; funding acquisition, S.N. All authors have read and agreed to the published version of the manuscript.

Institutional Review Board Statement

Not applicable.

Informed Consent Statement

Not applicable.

Data Availability Statement

Data supporting the findings of this study are available upon reasonable request from the corresponding author.

Funding

This research received no external funding.

Acknowledgments

The author wishes to express gratitude to the Dean of the Faculty of Health Sciences at Almarisah Madani University for offering the necessary facilities. Additionally, the author extends sincere appreciation to the members of the Kersen Research Team (Mulpi Alpia (M.A) and Jhaniartika Limbong (J.L)) for their valuable contributions to this study.

Conflicts of Interest

The authors declare no conflict of interest.

References

1. Wenas, D.M.; Elya, B.; Sutriyo, S.; Setiawan, H.; Othman, R.; Nur, S.; Triadisti, N.; Yunita, F.; Setyaningsih, E.P. In Vitro and In Silico Evaluation of the Anti-Aging Potential of Eugenia Uniflora UAE Extracts. *Molecules* **2025**, *30*, 3168, https://doi:10.3390/molecules30153168.
2. Shin, J.W.; Kwon, S.H.; Choi, J.Y.; Na, J.I.; Huh, C.H.; Choi, H.R.; Park, K.C. Molecular Mechanisms of Dermal Aging and Antiaging Approaches. *Int. J. Mol. Sci.* **2019**, *20*, https://doi:10.3390/ijms20092126.
3. Nur, S.; Hanafi, M.; Setiawan, H.; Elya, B. Chemical Characterization and Biological Activity of Molineria Latifolia Root Extract as Dermal Antiaging: Isolation of Natural Compounds, in Silico and in Vitro Study. *Biocatal. Agric. Biotechnol.* **2024**, 103039, https://doi.org/10.1016/j.bcab.2024.103039.
4. Nur, S.; Hanafi, M.; Setiawan, H.; Sami, F.J.; Elya, B. Biological Activity of Curculigo Latifolia Extract as Skin Antiaging: In Vitro and Silico Studies Approach. *Res. J. Pharm. Technol.* **2025**, *18*, 980–992, https://doi:10.52711/0974-360X.2025.00141.
5. Nur, S.; Sami, F.J.; Sapra, A.; Aisyah, A.N.; Burhan, A.; Megawati; Marwati; Yusuf, N.A.; Mislia; Nursamsiar Application Box Behnken Design for the Optimum Cream Formula of M. Calabura Fruit Extract: In Vitro and In Vivo Studies as an Antiaging Product. *Res. J. Pharm. Technol.* **2024**, *17*, 5325–5335, https://doi:10.52711/0974-360X.2024.00815.
6. Wu, S.; Zhou, X.; Jin, Z.; Cheng, H. Collagenases and Their Inhibitors: A Review. *Collagen and Leather* **2023**, *5*, 19, https://doi:10.1186/s42825-023-00126-6.
7. Pittayapruek, P.; Meephansan, J.; Prapapan, O.; Komine, M.; Ohtsuki, M. Role of Matrix Metalloproteinases in Photoaging and Photocarcinogenesis. *Int. J. Mol. Sci.* **2016**, *17*, 868, https://doi.org/10.3390/ijms17060868.
8. Lukitaningsih, E.; Nur, S.; Qonithah, F.; Zulbayu, A.; Kuswahyuning, R.; Rumiyati, R. *In Vitro* Anti-Wrinkle and Tyrosinase Inhibitory Activities of Grapefruit Peel and Strawberry Extracts. *Majalah Obat Tradisional* **2020**, *25*, 1–9, https://doi.org/10.22146/mot.59194.
9. Oh, Y.S.; Shin, S.Y.; Kim, S.; Lee, K.H.; Shin, J.C.; Park, K.M. Comparison of Antiaging, Anti-Melanogenesis Effects, and Active Components of Raspberry (*Rubus occidentalis* L.) Extracts According to Maturity. *J. Food Biochem.* **2020**, *44*, e13464, https://doi.org/10.1111/jfbc.13464.
10. Tsuji, N.; Moriwaki, S.; Suzuki, Y.; Takema, Y.; Imokawa, G. The Role of Elastases Secreted by Fibroblasts in Wrinkle Formation: Implication Through Selective Inhibition of Elastase Activity. *Photochem. Photobiol.* **2001**, *74*, 283–289, https://doi.org/10.1562/0031-8655(2001)074.
11. Nur, S.; Setiawan, H.; Hanafi, M.; Elya, B. Phytochemical Composition, Antioxidant, In Vitro and In Silico Studies of Active Compounds of Curculigo Latifolia Extracts as Promising Elastase Inhibitor. *Saudi J. Biol. Sci.* **2023**, *30*, 103716, https://10.1016/j.sjbs.2023.103716.
12. Buhren, B.A.; Schrumpf, H.; Hoff, N.P.; Bölke, E.; Hilton, S.; Gerber, P.A. Hyaluronidase: From Clinical Applications to Molecular and Cellular Mechanisms. *Eur. J. Med. Res.* **2016**, *21*, 5, https://doi.org/10.1186/s40001-016-0201-5.
13. He, X.; Wan, F.; Su, W.; Xie, W. Research Progress on Skin Aging and Active Ingredients. *Molecules* **2023**, *28*, 1803, https://doi.org/10.3390/molecules28041803
14. Anonymous. Gateway to Global Aging Data. Available online: https://g2aging.org/ (accessed on 16 November 2025).
15. Mahmood, N.D.; Nasir, N.L.M.; Rofiee, M.S.; Tohid, S.F.M.; Ching, S.M.; Teh, L.K.; Salleh, M.Z.; Zakaria, Z.A. Muntingia Calabura: A Review of Its Traditional Uses, Chemical Properties, and Pharmacological Observations. *Pharm. Biol.* **2014**, *52*, 1598–1623, https://10.3109/13880209.2014.908397.
16. Mastuki, S.N.; Faudzi, S.M.M.; Ismail, N.; Saad, N. *Muntingia calabura*: Chemical Composition, Bioactive Component and Traditional Uses. In *Wild Fruits: Composition, Nutritional Value and Products*; Mariod, A.A., Ed.; Springer International Publishing: Cham, Switzerland, **2019**; pp. 549–564.
17. Nur, S.; Aswad, M.; Yulianti, R.; Sami, F.J.; Burhan, A.; Fadri, A.; Khairi, N.; Nursamsiar. Antioxidant Activity Profile of Extract and Fraction of Kersen (*Muntingia calabura* L.) Fruits Prepared by Different Methods. In *Proceedings of the IOP Conference Series: Earth and Environmental Science*; IOP Publishing: Bristol, UK, **2022**; *1039*, 012034, https://doi.org/10.1088/1755-1315/1039/1/012034.
18. Nur, S.; Aisyah, A.; Nursamsiar, N.; Sami, F.; Fadri, A.; Khairi, N.; Sapra, A. Standardization and GC–MS Analysis of Kersen (*Muntingia calabura* L.) Fruit Ethanol Extract as an Herbal Raw Material. *Bull. Pharm. Sci. Assiut* **2023**, *46*, 185037, https://doi.org/10.21608/bfsa.2023.185037.1631.

19. Nur, S.; Angelina, A.A.; Aswad, M.; Yulianty, R.; Burhan, A.; Nursamsiar. *In Vitro* Anti-Aging Activity of *Muntingia calabura* L. Fruit Extract and Its Fractions. *J. Pharm. Pharmacogn. Res.* **2021**, *9*, 1–10, https://doi.org/10.56499/jppres21.9.1.001.
20. Nur, S.; Aisyah, A.; Burhan, A.; Sami, F.; Nursamsiar, N.; Sapra, A.; Megawati, M. Authentication of Cherry (*Muntingia calabura*) Fruit from Different Geographical Locations in Indonesia by FTIR Spectroscopy Combined with Chemometrics and Their Antioxidant and Antiaging Activities. *Egypt. J. Chem.* **2022**, *65*, 7079, https://doi.org/10.21608/ejchem.2022.168226.7079.
21. Nur, S.; Alwani, M.F.N.; Sami, F.J.; Sapra, A.; Aisyah, A.N.; Indrisari, M.; Nursamsiar; Yusuf, N.A.; Aristianti. Transfersome-Based Delivery of *Muntingia calabura* Fruit Extract for Anti-Aging Applications. *Biocatal. Agric. Biotechnol.* **2025**, *66*, 103604, https://doi.org/10.1016/j.bcab.2025.103604
22. Qiao, X.; Li, R.; Song, W.; Miao, W.; Liu, J.; Chen, H.; Guo, D.; Ye, M. A Targeted Strategy to Analyze Untargeted Mass Spectral Data: Rapid Chemical Profiling of *Scutellaria baicalensis* Using Ultra-High Performance Liquid Chromatography Coupled with Hybrid Quadrupole Orbitrap Mass Spectrometry and Key Ion Filtering. *J. Chromatogr. A* **2016**, *1441*, 83–95, https://doi.org/10.1016/j.chroma.2016.02.079.
23. Aristianti; Aswad, M.; Arsyad, A.; Nursamsiar; Nur, S.; Islam, A.A. The Potential Combination of *Centella asiatica*, *Curcuma longa*, and *Piper nigrum* Extracts in Treating Brain Injury: *In Vitro*, *In Vivo* and *In Silico* Studies. *Int. J. Appl. Pharm.* **2025**, *17*, 1–10, https://doi.org/10.22159/ijap.2025.v17i1.12345.
24. Xiong, G.; Wu, Z.; Yi, J.; Fu, L.; Yang, Z.; Hsieh, C.; Yin, M.; Zeng, X.; Wu, C.; Lu, A.; *et al*. ADMETlab 2.0: An Integrated Online Platform for Accurate and Comprehensive Predictions of ADMET Properties. *Nucleic Acids Res.* **2021**, *49*, W5–W14, https://doi.org/10.1093/nar/gkab255.
25. Mohamaden, Y.M.; El-Hawary, S.S.; El Fakharany, E.M.; El Maradny, Y.A.; Raey, M. El; El Senousy, A.S.; Bassam, S.M. Network Pharmacology of Olive Stem Extract, UPLC-HR-QTOF-MS Profiling and Antiviral Activities Aligned with UN Sustainable Development Goals. *Sci. Rep.* **2025**, *15*, 23665, https://doi.org/10.1038/s41598-025-07452-1.
26. Nursamsiar, N.; Sami, F.J.; Kasmawati, H.; Nur, S.; Marwati. Antioxidant Capacity, Inhibitor of Alpha-Glucosidase and DPP-IV of *Schleichera oleosa* Leaf Extract and Their Compound Profiles Based on LC-ESI-MS Analysis: *In Vitro* and *In Silico* Study. *Biointerface Res. Appl. Chem.* **2025**, *15*, 3037–3047, https://doi.org/10.33263/BRIAC153.037.
27. Sari, R.; Rahmasari, R.; Nur, S.; Elya, B. LC–MS/MS Analysis and Evaluation of Antibacterial Activity of *Curculigo latifolia* Extracts. *Int. J. Agric. Biol.* **2025**, *34*, 2341, https://doi.org/10.17957/IJAB/15.2341
28. Nur, S.; Hanafi, M.; Setiawan, H.; Nursamsiar, N.; Elya, B. *In Silico* Evaluation of the Dermal Antiaging Activity of *Molineria latifolia*. *J. Pharm. Pharmacogn. Res.* **2023**, *11*, 325–345, https://doi.org/10.56499/jppres23.11.325.
29. Kuriata, A.; Gierut, A.M.; Oleniecki, T.; Ciemny, M.P.; Kolinski, A.; Kurcinski, M.; Kmiecik, S. CABS-Flex 2.0: A Web Server for Fast Simulations of Flexibility of Protein Structures. *Nucleic Acids Res.* **2018**, *46*, W338–W343, https://doi.org/10.1093/nar/gky356.
30. López-Blanco, J.R.; Aliaga, J.I.; Quintana-Ortí, E.S.; Chacón, P. iMODS: Internal Coordinates Normal Mode Analysis Server. *Nucleic Acids Res.* **2014**, *42*, W271–W276, https://doi.org/10.1093/nar/gku339.
31. Zaib, S.; Rana, N.; Areeba; Hussain, N.; Alrbyawi, H.; Dera, A.A.; Khan, I.; Khalid, M.; Khan, A.; Al-Harrasi, A. Designing Multi-Epitope Monkeypox Virus-Specific Vaccine Using Immunoinformatics Approach. *J. Infect. Public Health* **2023**, *16*, 107–116, https://doi.org/10.1016/j.jiph.2022.11.033.
32. Ragasa, C.Y.; Tan, M.C.S.; Chiong, I.D.; Shen, C.C. Chemical Constituents of *Muntingia calabura* L. *Philipp. J. Sci.* **2015**, *144*, 1–8, https://doi.org/10.1007/pjs.2015.144.1.8.
33. López, A.; De Tangil, M.S.; Vega-Orellana, O.; Ramírez, A.S.; Rico, M. Phenolic Constituents, Antioxidant and Preliminary Antimycoplasmic Activities of Leaf Skin and Flowers of *Aloe vera* (L.) Burm. f. (Syn. *A. barbadensis* Mill.) from the Canary Islands (Spain). *Molecules* **2013**, *18*, 4942–4954, https://doi.org/10.3390/molecules18054942 .
34. Yong, H.J.; Ahn, J.J. Antioxidant and Skin Protection Effect of Morin upon UVA Exposure. *Biomed. Dermatol.* **2018**, *2*, 26–33, https://doi.org/10.1186/s41702-018-0026-7.
35. Jung, S.K.; Lee, K.W.; Kim, H.Y.; Oh, M.H.; Byun, S.; Lim, S.H.; Heo, Y.S.; Kang, N.J.; Bode, A.M.; Dong, Z.; *et al*. Myricetin Suppresses UVB-Induced Wrinkle Formation and MMP-9 Expression by Inhibiting Raf. *Biochem. Pharmacol.* **2010**, *79*, 1455–1461, https://doi.org/10.1016/j.bcp.2010.01.004.

36. Zhang, Z.; Bian, Q.; Luo, P.; Sun, W. Ethnopharmacological, Chemical, and Pharmacological Aspects of *Halenia elliptica*: A Comprehensive Review. *Pharmacogn. Rev.* **2015**, *9*, 114–119, https://doi.org/10.4103/0973-7847.162103.
37. Huang, B.; Ke, H.; He, J.; Ban, X.; Zeng, H.; Wang, Y. Extracts of *Halenia elliptica* Exhibit Antioxidant Properties *In Vitro* and *In Vivo*. *Food Chem. Toxicol.* **2011**, *49*, 185–190, https://doi.org/10.1016/j.fct.2010.10.015.
38. Huang, B.; Ban, X.; He, J.; Zeng, H.; Zhang, P.; Wang, Y. Hepatoprotective and Antioxidant Effects of the Methanolic Extract from *Halenia elliptica*. *J. Ethnopharmacol.* **2010**, *131*, 276–281, https://doi.org/10.1016/j.jep.2010.06.029.
39. Ağalar, H.G.; İşcan, G.; Noma, Y.; Atlı, Ö.; Demirci, F.; Kırımer, N. Biological Evaluation of 2,5-Dimethyl-1,4-Benzoquinone Biotransformation Metabolite. *Nat. Prod. Commun.* **2017**, *4*, 1–6, https://doi.org/10.1177/1934578X1701200403.
40. Zhou, Y.F.; Qi, J.; Zhu, D.N.; Yu, B.Y. Homoisoflavonoids from *Ophiopogon japonicus* and Their Oxygen Free Radical Scavenging Effects. *Chin. J. Nat. Med.* **2008**, *6*, 201–204, https://doi.org/10.1016/S1875-5364(09)60017-0.
41. Mendez-Callejas, G.; Piñeros-Avila, M.; Celis, C.A.; Torrenegra, R.; Espinosa-Benitez, A.; Pestana-Nobles, R.; Yosa-Reyes, J. Natural 2′,4-Dihydroxy-4′,6′-Dimethoxy Chalcone Isolated from *Chromolaena tacotana* Inhibits Breast Cancer Cell Growth through Autophagy and Mitochondrial Apoptosis. *Plants* **2024**, *13*, 570, https://doi.org/10.3390/plants13050570.
42. Teerapongpisan, P.; Praparatana, R.; Noppradit, B.; Laphookhieo, S.; Puttarak, P. Anti-Diabetic Compounds from *Uvaria dulcis* Dunal. *Heliyon* **2024**, *10*, e26962, https://doi.org/10.1016/j.heliyon.2024.e26962.
43. Chan, Y.S.; Wang, J.P.; Chen, S.C.; Kuo, S.C. Three New Flavonoids and Antiallergic, Anti-Inflammatory Constituents from the Heartwood of *Dalbergia odorifera*. *Planta Med.* **1998**, *64*, 153–158, https://doi.org/10.1055/s-2006-957394.
44. Yokosuka, A.; Tatsuno, S.; Komine, T.; Mimaki, Y. Chemical Constituents of the Roots and Rhizomes of *Saposhnikovia divaricata* and Their Cytotoxic Activity. *Nat. Prod. Commun.* **2017**, *12*, 255–258, https://doi.org/10.1177/1934578X1701200405.
45. Jan, K.C.; Gavahian, M. Hydroxylated Tetramethoxyflavone Affects Intestinal Cell Permeability and Inhibits Cytochrome P450 Enzymes. *Molecules* **2024**, *29*, 322, https://doi.org/10.3390/molecules29020322.
46. Sharma, S.; Patial, V.; Singh, D.; Sharma, U.; Kumar, D. Antimicrobial Homoisoflavonoids from the Rhizomes of *Polygonatum verticillatum*. *Chem. Biodivers.* **2018**, *15*, e1800430, https://doi.org/10.1002/cbdv.201800430.
47. Wang, D.; Zeng, L.; Li, D.; Pu, W. Antioxidant Activities of Different Extracts and Homoisoflavanones Isolated from *Polygonatum odoratum*. *Nat. Prod. Res.* **2013**, *27*, 1111–1114, https://doi.org/10.1080/14786419.2012.701212.
48. Filho, A.; Fernandes, H.; Sousa, J.; Maia, G.; Filho, J.; Assis, T.; Pêssoa, H.; Lima, E. Antifungal Effect of Flavonoid 5,7,4′-Trimethoxyflavone against *Candida krusei* Strains. *Int. J. Trop. Dis. Health* **2015**, *5*, 136–140, https://doi.org/10.9734/ijtdh/2015/14060.
49. Wang, Q.; Luo, J.; Liu, H.; Brennan, C.S.; Liu, J.; Zou, X. Protective Effects of the Flavonoid Fraction Obtained from Pomelo Fruitlets through Ultrasonic-Associated Microwave Extraction against AAPH-Induced Erythrocyte Hemolysis. *RSC Adv.* **2019**, *9*, 16007–16017, https://doi.org/10.1039/c9ra02523e.
50. Roshni, J.; Ahmad, S.F.; Wani, A.; Ahmed, S.S.S.J. Multi-Target Effect of Aloeresin-A against Bacterial and Host Inflammatory Targets Benefits Contact Lens-Related Keratitis: A Multi-Omics and Quantum Chemical Investigation. *Molecules* **2023**, *28*, 6955, https://doi.org/10.3390/molecules28196955.
51. Mikayoulou, M.; Mayr, F.; Temml, V.; Pandian, A.; Vermaak, I.; Chen, W.; Komane, B.; Stuppner, H.; Viljoen, A. Anti-Tyrosinase Activity of South African *Aloe* Species and Isolated Compounds Plicataloside and Aloesin. *Fitoterapia* **2021**, *150*, 104828, https://doi.org/10.1016/j.fitote.2021.104828.
52. Jong-Anurakkun, N.; Bhandari, M.R.; Hong, G.; Kawabata, J. α-Glucosidase Inhibitor from Chinese Aloes. *Fitoterapia* **2008**, *79*, 456–457, https://doi.org/10.1016/j.fitote.2008.02.010.
53. Sattar, M.; Saeed, F.; Afzaal, M.; Rasheed, A.; Asif, A.; Sharif, S.; Hussain, M.; Rehman, H.A.U.; Raza, M.A.; Munir, H.; *et al*. An Overview of the Nutritional and Therapeutic Properties of Amaranth. *Int. J. Food Prop.* **2024**, *27*, 263–272, https://doi.org/10.1080/10942912.2024.1234567.

54. Baig, M.M.V. Phytochemical and Antimicrobial Activity Screening of Seeds of *Psoralea corylifolia* L. *Phytomedicine Plus* **2022**, *2*, 100278, https://doi.org/10.1016/j.phyplu.2022.100278.
55. Zhang, B.; Zhao, J.; Wang, Z.; Guo, P.; Liu, A.; Du, G. Identification of Multi-Target Anti-AD Chemical Constituents from Traditional Chinese Medicine Formulae by Integrating Virtual Screening and *In Vitro* Validation. *Front. Pharmacol.* **2021**, *12*, 709607, https://doi.org/10.3389/fphar.2021.709607.
56. Han, M.; Du, W.; Zhang, L.; Wang, Z.; Fang, S.; Zheng, Y.; Quan, R. Dichotomitin Promotes Osteoblast Differentiation and Improves Osteoporosis by Inhibiting Oxidative Stress. *J. Orthop. Surg. Res.* **2025**, *20*, 5398, https://doi.org/10.1186/s13018-024-05398-0.
57. Chou, C.H.; Hsu, K.C.; Lin, T.E.; Yang, C.R. Anti-Inflammatory and Tau Phosphorylation-Inhibitory Effects of Eupatin. *Molecules* **2020**, *25*, 5652, https://doi.org/10.3390/molecules25235652.
58. Park, Y.I.; Kim, J.H.; Lee, S.; Lee, I.S.; Park, J. Eupatin, a Flavonoid, Inhibits Coronavirus 3CL Protease and Replication. *Int. J. Mol. Sci.* **2023**, *24*, 19211, https://doi.org/10.3390/ijms24119211
59. Pan, Y.; Zhao, Y.L.; Zhang, J.; Li, W.Y.; Wang, Y.Z. Phytochemistry and Pharmacological Activities of the Genus *Gentiana* (Gentianaceae). *Chem. Biodivers.* **2016**, *13*, 107–150, https://doi.org/10.1002/cbdv.201500333.
60. Qian, W.; Lu, J.; Gao, C.; Liu, Q.; Yao, W.; Wang, T.; Wang, X.; Wang, Z. Isobavachalcone Exhibits Antifungal and Antibiofilm Effects against *Candida albicans* by Disrupting Cell Wall/Membrane Integrity and Inducing Apoptosis and Autophagy. *Front. Cell. Infect. Microbiol.* **2024**, *14*, 1336773, https://doi.org/10.3389/fcimb.2024.1336773.
61. Li, S.; Wang, S.; Zhang, L.; Ka, Y.; Zhou, M.; Wang, Y.; Tang, Z.; Zhang, J.; Wang, W.; Liu, W. Research Progress on Pharmacokinetics, Anti-Inflammatory and Immunomodulatory Effects of Kaempferol. *Int. Immunopharmacol.* **2025**, *152*, 114387, https://doi.org/10.1016/j.intimp.2025.114387.
62. Jin, S.; Zhang, L.; Wang, L. Kaempferol, a Potential Neuroprotective Agent in Neurodegenerative Diseases: From Chemistry to Medicine. *Biomed. Pharmacother.* **2023**, *165*, 115215, https://doi.org/10.1016/j.biopha.2023.115215.
63. Lin, C.F.; Lin, M.H.; Hung, C.F.; Alshetaili, A.; Tsai, Y.F.; Jhong, C.L.; Fang, J.Y. The Anti-Inflammatory Activity of Flavonoids and Alkaloids from *Sophora flavescens* Alleviates Psoriasiform Lesions: Prenylation and Methoxylation Beneficially Enhance Bioactivity and Skin Targeting. *Phytother. Res.* **2024**, *38*, 1951–1970, https://doi.org/10.1002/ptr.8140.
64. Yang, Y.; Wang, S.; Bao, Y.; Li, T.; Yang, G.; Chang, X.; Meng, X. Anti-Ulcer Effect and Potential Mechanism of Licoflavone by Regulating Inflammation Mediators and Amino Acid Metabolism. *J. Ethnopharmacol.* **2017**, *199*, 175–182, https://doi.org/10.1016/j.jep.2017.01.053.
65. Lee, A.; Kwon, H.; Kim, S.; Jeong, Y.; Choi, B.T.; Kho, C. Protective Effect of Maltol on Pathological Response of Cardiomyocyte in Dystrophic Mice. *Korean J. Physiol. Pharmacol.* **2025**, *29*, 235–244, https://doi.org/10.4196/kjpp.24.246.
66. Ziklo, N.; Bibi, M.; Salama, P. The Antimicrobial Mode of Action of Maltol and Its Synergistic Efficacy with Selected Cationic Surfactants. *Cosmetics* **2021**, *8*, 86, https://doi.org/10.3390/cosmetics8030086.
67. Lin, M.; Sun, W.; Gong, W.; Zhou, Z.; Ding, Y.; Hou, Q. Methylophiopogonanone A Protects against Cerebral Ischemia/Reperfusion Injury and Attenuates Blood-Brain Barrier Disruption *In Vitro*. *PLoS One* **2015**, *10*, e0124558, https://doi.org/10.1371/journal.pone.0124558.
68. Goyal, A.; Dubey, N.; Agrawal, A.; Verma, A.; Sharma, R. Therapeutic Potential of Morin: Special Focus on Cognitive Dysfunction, Diabetes Mellitus and Cancer. *Pharmacol. Res. Mod. Chin. Med.* **2023**, *9*, 100318, https://doi.org/10.1016/j.prmcm.2023.100318.
69. Park, K.S.; Chong, Y.; Kim, M.K. Myricetin: Biological Activity Related to Human Health. *Appl. Biol. Chem.* **2016**, *59*, 259–269, https://doi.org/10.1007/s13765-016-0154-3.
70. Wang, Y.Q.; Weng, Z.M.; Dou, T.Y.; Hou, J.; Wang, D.D.; Ding, L.L.; Zou, L.W.; Yu, Y.; Chen, J.; Tang, H.; *et al*. Nevadensin Is a Naturally Occurring Selective Inhibitor of Human Carboxylesterase 1. *Int. J. Biol. Macromol.* **2018**, *120*, 1944–1954, https://doi.org/10.1016/j.ijbiomac.2018.09.178.
71. Huang, H.; Li, L.; Shi, W.; Liu, H.; Yang, J.; Yuan, X.; Wu, L. The Multifunctional Effects of Nobiletin and Its Metabolites *In Vivo* and *In Vitro*. *Evid.-Based Complement. Altern. Med.* **2016**, *2016*, 1–12, https://doi.org/10.1155/2016/1234567.
72. Kitahiro, Y.; Shibano, M. Antioxidant Properties and Applications of *Ophiopogon japonicus* Root for Age-Related Disease. In *Aging*, 2nd ed.; Preedy, V.R., Patel, V.B., Eds.; Academic Press: London, UK, **2020**; pp. 275–282, ISBN 978-0-12-818698-5, https://doi.org/10.1016/B978-0-12-818698-5.00027-8.

73. Kitahiro, Y.; Koike, A.; Sonoki, A.; Muto, M.; Ozaki, K.; Shibano, M. Anti-Inflammatory Activities of *Ophiopogonis radix* on Hydrogen Peroxide-Induced Cellular Senescence of Normal Human Dermal Fibroblasts. *J. Nat. Med.* **2018**, *72*, 905–914, https://doi.org/10.1007/s11418-018-1223-9.
74. Amini, A.M.; Muzs, K.; Spencer, J.P.E.; Yaqoob, P. Pelargonidin-3-O-Glucoside and Its Metabolites Have Modest Anti-Inflammatory Effects in Human Whole Blood Cultures. *Nutr. Res.* **2017**, *46*, 88–95, https://doi.org/10.1016/j.nutres.2017.09.006
75. Endo, K.; Matsui, R.; Sugiyama, M.; Asami, T.; Inaba, C.; Kobayashi, S.; Makabe, H.; Tanaka, S. Procyanidin B2 Gallate Regulates TNF-α Production from T Cells through Inhibiting Glycolytic Activity via mTOR-HIF-1 Pathway. *Biochem. Pharmacol.* **2020**, *177*, 113952, https://doi.org/10.1016/j.bcp.2020.113952.
76. Ferreira, J.F.S.; Luthria, D.L.; Sasaki, T.; Heyerick, A. Flavonoids from *Artemisia annua* L. as Antioxidants and Their Potential Synergism with Artemisinin against Malaria and Cancer. *Molecules* **2010**, *15*, 3135–3170, https://doi.org/10.3390/molecules15043135.
77. Mao, H.; Feng, Y.; Feng, J.; Yusufu, Y.; Sun, M.; Yang, L.; Jiang, Q. Quercetin-3-O-β-D-Glucuronide Attenuates Osteoarthritis by Inhibiting Cartilage Extracellular Matrix Degradation and Inflammation. *J. Orthop. Transl.* **2024**, *45*, 236–246, https://doi.org/10.1016/j.jot.2024.01.007.
78. Hu, Y.K.; Liu, Y.M.; Bai, X.L.; Ma, C.; Liao, X. Screening of Monoamine Oxidase B Inhibitors from *Fragaria nubicola* by Ligand Fishing and Their Neuroprotective Effects. *J. Agric. Food Chem.* **2023**, *71*, 512–521, https://doi.org/10.1021/acs.jafc.2c06630.
79. Shahidi, F.; Ambigaipalan, P. Phenolics and Polyphenolics in Foods, Beverages and Spices: Antioxidant Activity and Health Effects—A Review. *J. Funct. Foods* **2015**, *18*, 820–897, https://doi.org/10.1016/j.jff.2015.06.018.
80. Rusu, M.E.; Fizeșan, I.; Vlase, L.; Popa, D.S. Antioxidants in Age-Related Diseases and Anti-Aging Strategies. *Antioxidants* **2022**, *11*, 1234, https://doi.org/10.3390/antiox11061234.
81. Kim, M.; Park, H.J. Molecular Mechanisms of Skin Aging and Rejuvenation. In *Molecular Mechanisms of the Aging Process and Rejuvenation*; IntechOpen: London, UK, **2016**; https://doi.org/10.5772/62983
82. Shin, J.W.; Kwon, S.H.; Choi, J.Y.; Na, J.I.; Huh, C.H.; Choi, H.R.; Park, K.C. Molecular Mechanisms of Dermal Aging and Antiaging Approaches. *Int. J. Mol. Sci.* **2019**, *20*, 2126, https://doi.org/10.3390/ijms20092126.
83. Lipinski, C.A. Lead- and Drug-Like Compounds: The Rule-of-Five Revolution. *Drug Discov. Today Technol.* **2004**, *1*, 337–341, https://doi.org/10.1016/j.ddtec.2004.11.007.
84. El-Kattan, A.F. Physicochemical and Biopharmaceutical Properties That Affect Drug Absorption of Compounds Absorbed by Passive Diffusion. In *Oral Bioavailability Assessment*; Li, X., Ed.; Wiley: Hoboken, NJ, USA, **2017**; pp. 139–171, ISBN 9781118916926, https://doi.org/10.1002/9781118916926.ch7.
85. Leite-Silva, V.R.; de Almeida, M.M.; Fradin, A.; Grice, J.E.; Roberts, M.S. Delivery of Drugs Applied Topically to the Skin. *Expert Rev. Dermatol.* **2012**, *7*, 383–397, https://doi.org/10.1586/edm.12.32
86. Li, X.; Li, C.; Zhang, W.; Wang, Y.; Qian, P.; Huang, H. Inflammation and Aging: Signaling Pathways and Intervention Therapies. *Signal Transduct. Target. Ther.* **2023**, *8*, 1502, https://doi.org/10.1038/s41392-023-01502-8.
87. Hwang, B.M.; Noh, E.M.; Kim, J.S.; Kim, J.M.; Hwang, J.K.; Kim, H.K.; Kang, J.S.; Kim, D.S.; Chae, H.J.; You, Y.O.; *et al*. Decursin Inhibits UVB-Induced MMP Expression in Human Dermal Fibroblasts via Regulation of Nuclear Factor-κB. *Int. J. Mol. Med.* **2013**, *31*, 1202–1210, https://doi.org/10.3892/ijmm.2012.1202.
88. Shen, J.; Wang, Z.; Zhao, W.; Fu, Y.; Li, B.; Cheng, J.; Deng, Y.; Li, S.; Li, H. TGF-β1 Induces Type I Collagen Deposition in Granulosa Cells via the AKT/GSK-3β Signaling Pathway-Mediated MMP1 Down-Regulation. *Reprod. Biol.* **2022**, *22*, 100705, https://doi.org/10.1016/j.repbio.2022.100705.
89. Cho, J.H.; Song, M.C.; Lee, Y.; Noh, S.T.; Kim, D.O.; Rha, C.S. Newly Identified Maltol Derivatives in Korean Red Ginseng and Their Biological Influence as Antioxidant and Anti-Inflammatory Agents. *J. Ginseng Res.* **2023**, *47*, 593–603, https://doi.org/10.1016/j.jgr.2023.02.006.
90. Forli, S.; Huey, R.; Pique, M.E.; Sanner, M.F.; Goodsell, D.S.; Olson, A.J. Computational Protein-Ligand Docking and Virtual Drug Screening with the AutoDock Suite. *Nat. Protoc.* **2016**, *11*, 905–919, https://doi.org/10.1038/nprot.2016.051.
91. Pantsar, T.; Poso, A. Binding Affinity via Docking: Fact and Fiction. *Molecules* **2018**, *23*, 1899, https://doi.org/10.3390/molecules23081899.

92. Kim, H.; Choi, J.; Lee, H.; Park, J.; Yoon, B.I.; Jin, S.M.; Park, K. Skin Corrosion and Irritation Test of Nanoparticles Using Reconstructed Three-Dimensional Human Skin Model, EpiDerm™. *Toxicol. Res.* **2016**, *32*, 311–316, https://doi.org/10.5487/TR.2016.32.4.311.
93. López-Blanco, J.R.; Garzón, J.I.; Chacón, P. iMod: Multipurpose Normal Mode Analysis in Internal Coordinates. *Bioinformatics* **2011**, *27*, 2843–2850, https://doi.org/10.1093/bioinformatics/btr497.
94. Putra, P.P.; Armin, F.; Florida, N.; Yusuf, G.V.; Suharti, N. Molecular Dynamics, Prediction of Toxicity, and Interaction of the Active Compound *Caesalpinia sappan* on Essential Lipids of *Klebsiella pneumoniae*. In *Proceedings of the 2nd International Conference on Contemporary Science and Clinical Pharmacy (ICCSCP 2021)*; Atlantis Press: Paris, France, 2022; Vol. 40, pp. 1–6.
95. Sumera; Anwer, F.; Waseem, M.; Fatima, A.; Malik, N.; Ali, A.; Zahid, S. Molecular Docking and Molecular Dynamics Studies Reveal Secretory Proteins as Novel Targets of Temozolomide in Glioblastoma Multiforme. *Molecules* **2022**, *27*, 7198, https://doi.org/10.3390/molecules27217198.
96. Sun, Z.; Liu, Q.; Qu, G.; Feng, Y.; Reetz, M.T. Utility of B-Factors in Protein Science: Interpreting Rigidity, Flexibility, and Internal Motion and Engineering Thermostability. *Chem. Rev.* **2019**, *119*, 1626–1665, https://doi.org/10.1021/acs.chemrev.8b00290.
97. Likhachev, I.V.; Balabaev, N.K.; Galzitskaya, O.V. Available Instruments for Analyzing Molecular Dynamics Trajectories. *Open Biochem. J.* **2016**, *10*, 1–11, https://doi.org/10.2174/1874091X01610010001.
98. Paul, S.K.; Saddam, M.; Rahaman, K.A.; Choi, J.G.; Lee, S.S.; Hasan, M. Molecular Modeling, Molecular Dynamics Simulation, and Essential Dynamics Analysis of Grancalcin: An Upregulated Biomarker in Experimental Autoimmune Encephalomyelitis Mice. *Heliyon* **2022**, *8*, e11232, https://doi.org/10.1016/j.heliyon.2022.e11232.

Publisher's Note & Disclaimer